Gold nanofilms at liquid-liquid interfaces: an emerging platform for redox electrocatalysis, nanoplasmonic sensors and electrovariable optics

Micheál D Scanlon, Evgeny Smirnov, Jane Talia Stockmann, Pekka Peljo

Gold nanofilms at liquid-liquid interfaces: an emerging platform for redox electrocatalysis, nanoplasmonic sensors and electrovariable optics

Micheál D. Scanlon,[1,*] Evgeny Smirnov,[2] T. Jane Stockmann[3] and Pekka Peljo[2]

[1]The Bernal Institute and Department of Chemical Sciences, School of Natural Sciences, University of Limerick (UL), Limerick V94 T9PX, Ireland.

[2]Laboratoire d'Electrochimie Physique et Analytique (LEPA), École Polytechnique Fédérale de Lausanne (EPFL), Rue de l'Industrie 17, CH-1951 Sion, Switzerland.

[3]Sorbonne Paris Cité, Paris Diderot University, Interfaces, Traitements, Organisation et Dynamique des Systèmes, CNRS-UMR 7086, 15 rue J.A. Baïf, 75013 Paris, France

*E-mail: micheal.scanlon@ul.ie, Telephone +353-61-237760.

Abstract

The functionality of liquid-liquid interfaces formed between two immiscible electrolyte solutions (ITIES) can be markedly enhanced by modification with supramolecular assemblies or solid nanomaterials. The focus of this review is recent progress involving ITIES modified with floating assemblies of gold nanoparticles or "nanofilms". Experimental methods to controllably modify liquid-liquid interfaces with gold nanofilms are detailed. Also, we outline an array of techniques to characterise these gold nanofilms in terms of their physiochemical properties (such as reflectivity, conductivity, catalytic activity or plasmonic properties) and physical interfacial properties (for example, interparticle spacing and immersion depth at the interface). The ability of floating gold nanofilms to impact a diverse range of fields is demonstrated, in particular redox electrocatalysis, surface-enhanced Raman spectroscopy (SERS) or surface plasmon resonance (SPR) based sensors, and electrovariable optical devices. Finally, perspectives on applications beyond the state-of-the-art are provided.

Keywords: Gold nanoparticles, nanofilms, interfaces, redox electrocatalysis, plasmonic properties

1. Introduction

Liquid-liquid interfaces are emerging as powerful transparent, defect-free platforms for bottom-up self-assembly of ordered two-dimensional (2D) and 3-dimensional (3D) gold nanoparticle (AuNP) arrays [1,2]. The fluidic nature of these interfaces allows them to self-heal, permitting the preparation of robust gold nanofilms of remarkable uniformity at room temperature, extending over large geometric areas (at least cm^2), without the use of specialist equipment [3]. The manipulation of the physical positions [4,5] and electrochemical activity [6–8] of the AuNPs within the nanofilm is possible by controllably applying an electric field across the liquid-liquid interface. Interfaces formed between two immiscible electrolyte solutions (ITIES) of either aqueous-organic solvent [9,10], aqueous-superhydrophobic ionic liquid [11] or organic solvent-ionic liquid phases [12] have the potential to support gold nanofilms. As ionic liquid-based ITIES have yet to be modified with gold nanofilms, this review will focus exclusively on aqueous-organic solvent ITIES.

2. The interface between two immiscible electrolyte solutions (ITIES)

The meaning of the word “immiscible” in the abbreviation of ITIES is multifaceted. The ITIES is firstly immiscible in terms of the solvent molecules, resulting in a molecularly sharp interface but with a dynamic microscopic roughness as “fingers” of the aqueous phase protrude into the organic solvent and *vice versa* [13]. Secondly, the ITIES is immiscible in terms of partition of the electrolyte ions between the two phases within a certain range of applied potential across the interface, known as the polarisable potential window (PPW).

As the acronym ITIES suggests, both phases conduct electricity by dissolution of electrolyte salts in either phase. At a liquid-liquid interface the maximum upper and lower potentials are limited by the transfer of the supporting electrolyte ions. Thus, to obtain a wide PPW, highly hydrophilic inorganic salts (*e.g.,* Li_2SO_4, KCl, *etc.*) are used in the aqueous phase and highly hydrophobic salts, typically composed of bulky organic ions such as bis(triphenylphosphoranylidene)ammonium cations (BA^+) and tetrakis(pentafluorophenyl)borate anions (TB^-) are employed in the organic phase. This means

that at high positive potentials the PPW is limited by aqueous cation transfer, while at negative potentials the aqueous anion limits the potential window (see **Fig. 1**); it has been shown that the organic phase electrolyte BATB contributes minimally [14–16]. Of course, supporting electrolyte of the organic phase can be chosen so that the ion transfer from the organic phase limits the potential window from one or both ends (for example replacement of TB^- with tetraphenylborate (TPB^-) would result in the positive end of the PPW being limited by transfer of TPB^- from organic to aqueous phase). A sufficiently polar organic solvent, typically 1,2-dichloroethane (DCE) [16], 1,2-dichlorobenzene (DCB) [17,18], or α,α,α-trifluorotoluene (TFT) [19], having relative permittivities (ε) of 10.4, 10.1, and 9.2, respectively, are often required to facilitate dissociation of the organic electrolyte salt as well as to support the flow of current. However, even chloroform [20,21] or toluene [22], which have low values of ε (4.8 and 2.4, respectively), can be used at micro-interfaces, where the low conductivity of the organic solvent is not such a significant issue. More polar water immiscible organic solvents have also been used, such as nitrobenzene (ε=34.8) [23]. Other highly polar organic solvents such as acetonitrile (ε = 36.6) [24,25] or propylene carbonate (ε = 66.1) [26] become immiscible with water if a heavy loading of supporting electrolyte is employed to force a phase separation. However, use of the latter two approaches results in a reduction in the overall size of the PPW as the solvation of ions is similar in both phases (the transfer energy of even highly hydrophilic and hydrophobic ions between phases is too close to 0 kJ mol^{-1} to allow separation of the waves). As a result neither are suitable to form an ITIES with a usable PPW. The discussion above is not an exhaustive account of all organic solvents used to form ITIES. For more options see the introduction of the article by Kasano *et al.* [22].

The ITIES can be controllably polarised, or electrified, by application of a potential, either externally through the use of electrodes immersed in either phase or through a common ion dissolved in both phases. The potential drop spans the interface and is termed the Galvani potential difference ($\phi_w - \phi_o = \Delta_o^w \phi$) and can be manipulated to provide a PPW as wide as ~1.0 V [9,10]. The width of the PPW is limited by the above factors (choice of supporting electrolyte, solvent, *etc.*). A typical 4-electrode electrochemical cell used to polarise an ITIES externally is shown in **Fig. 1**.

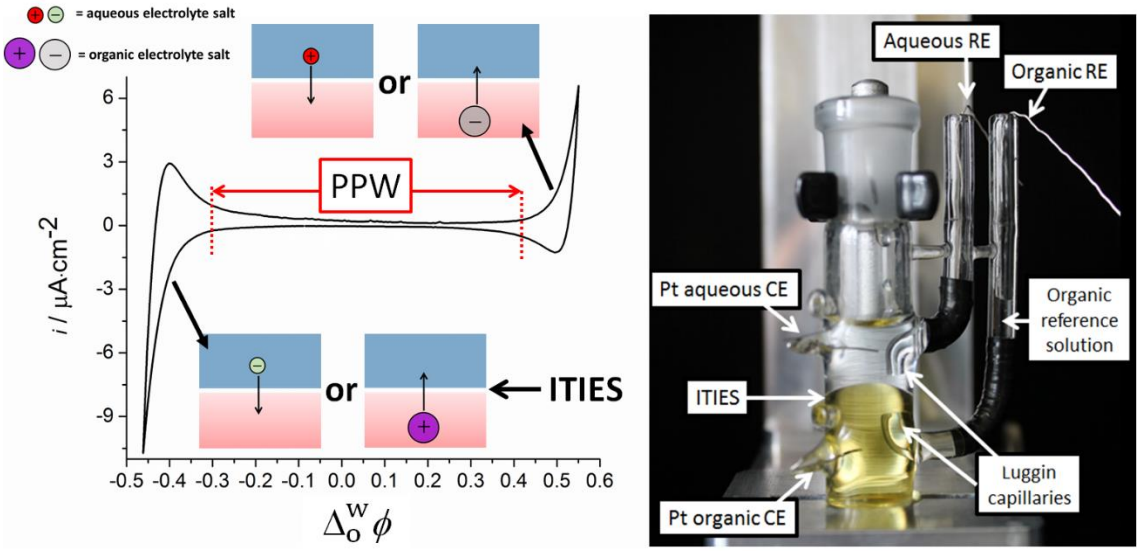

Fig. 1: Electrochemistry at the interface between two immiscible electrolyte solutions (ITIES). Note the water phase is blue and oil phase is red in this scheme. (**Left panel**) A typical cyclic voltammogram (CV) obtained by external polarisation of an ITIES using a potentiostat. At high positive potentials the polarisable potential window (PPW) is limited by aqueous cation transfer (*e.g.,* Li^+, Na^+ or Mg^{2+}) while at negative potentials the aqueous anion limits (*e.g.,* Cl–, or SO_4^{2-}). In theory, at very positive potentials the PPW may be limited by organic anion transfer, while at negative potentials the organic cation may limit. This is indeed the case if moderately hydrophobic salts such as tetrabutylammonium tetraphenylborate (TBATPB) are dissolved in the oil phase. However, with the extremely hydrophobic salt BATB is dissolved in the oil phase it has been shown that the organic phase electrolyte contributes minimally. (**Right panel**) A typical 4-electrode electrochemical cell used to polarise an ITIES externally is shown with two platinum (Pt) counter electrodes (CE), one in each phase, and two Ag/AgCl reference electrodes (RE), one in the aqueous phase and one in the organic reference solution (see the reviews listed in the text for more details on this solution). The dense halogenated solvent, in this case α,α,α-trifluorotoluene (TFT), is on the bottom and coloured yellow as ferrocene is dissolved in it to clarify the position of the ITIES in the image.

Taking into account the sharp thickness of the interfacial back-to-back diffuse electric double layers (ca. 1 nm) formed upon contacting two liquid electrolyte phases, very strong electric fields can be achieved (ca. 10^9 V/m). The majority of the potential drop takes place across these two double layers, in comparison to across just a single diffuse electric double layer built up at the surface of a polarised solid electrode. Indeed, a major distinguishing factor of electrochemistry at the ITIES is its sheer versatility in comparison to using solid electrodes,

encompassing ion transfer (IT; **Fig. 2A-B**) , facilitated ion transfer (FIT; **Fig. 2C**), interfacial electron transfer (IET; **Fig. 2D**) and photo-induced interfacial electron transfer (PET; **Fig. 2E**) processes. In-depth discussions of the theoretical background and plethora of possible applications of electrochemistry at the ITIES beyond the scope of this review are available in a series of recent reviews [9,10,27–31].

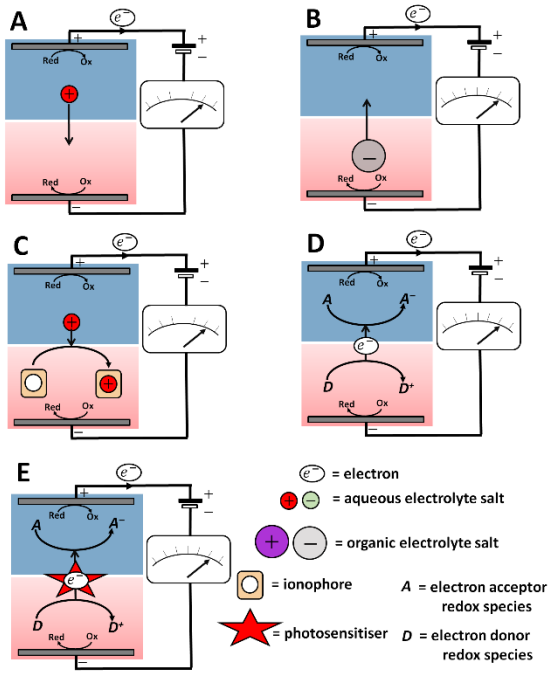

Fig. 2. The versatility of electrochemistry at the ITIES. In each of the schemes the ITIES is polarised positively by a potentiostat. Positive polarisation of the ITIES can lead to ion transfer (IT) within the PPW of (**A**) cations from the oil phase (red) to water phase (blue) or (**B**) anions from oil to water. (**C**) For very hydrophilic cations, facilitated ion transfer (FIT) can be achieved in the presence of a suitable ionophore species in the oil phase. Ionophores are complexing agents that can shift the apparent solvation energy, and are typically used to facilitate the transfer of very hydrophilic species from water to oil within the PPW. Positive polarisation of the ITIES can provide (**D**) a thermodynamic driving force for interfacial electron transfer (IET) from a hydrophobic electron donor redox couple, *D*, to a hydrophilic electron acceptor redox couple, *A*. In some instances, more driving force is required to achieve electron transfer across the ITIES, and this can be provided by (**E**) harvesting solar energy using photosensitisers immobilised at the ITIES (*e.g.,* porphyrins or semiconductors) in a process known as photo-induced electron transfer (PET). Negative polarisation of the ITIES may impede or reverse the direction of the charge transfer events described above.

3. Fundamental features of floating gold nanofilms that make them ideal for redox electrocatalysis, nanoplasmonic sensor and electrovariable optic applications

3.1 Redox electrocatalysis

As described in a recent review, electrocatalysis is catalysis of electron transfer at the electrode surface (catalysed by the electrode material itself or by a catalyst attached to the electrode surface), while redox electrocatalysis is catalysis of electron transfer between two redox couples, catalysed by a floating conductive catalyst [32]. Electrocatalysis and redox electrocatalysis are topics of pivotal importance impacting a huge variety of fields ranging from corrosion science, fuel cell and battery research, electro-organic synthesis, electroanalytical sensor development to waste-water purification [32,33]. To optimise the performance of nanoparticles towards electrocatalysis, a burgeoning area of research concerns support-induced effects [34,35]. For example, the supporting material for AuNPs can deeply affect their activities, as exhibited for AuNPs supported on carbon and on titania in the CO oxidation reaction [36].

Electrochemistry of catalytic interfacial gold nanofilms at the ITIES has several distinguishing features in comparison to electrochemical studies of AuNPs on solid electrode surfaces. Most strikingly, the electrocatalytic activity of interfacial adsorbed AuNPs can be studied in a "contactless" manner, free from the influence of an underlying support. Just as with solid electrodes, the ITIES allows direct measurement of the electrocatalytic impact of gold nanofilms by measurement of charge transfer across the interface corresponding to electron transfer events. At solid electrode interfaces the rate of an electrocatalysed reaction can be controlled by varying the electrode potential and concentration ratio of oxidised to reduced species initially present in solution (*i.e.,* two independent variables). Attractively, the ITIES has in fact three independent variables to study redox electrocatalysis: the ratio of oxidised to reduced species in (i) the aqueous phase and (ii) the organic phase, and (iii) the ability to manipulate $\Delta_{\mathrm{o}}^{\mathrm{w}}\phi$ externally with a potentiostat. Effectively, the AuNPs act as conductive bipolar electrodes facilitating catalysis *via* direct IET (through Fermi level equilibration [7,37]) between a lipophilic electron donor and a hydrophilic electron acceptor, or *vice versa* (see **Fig. 3**).

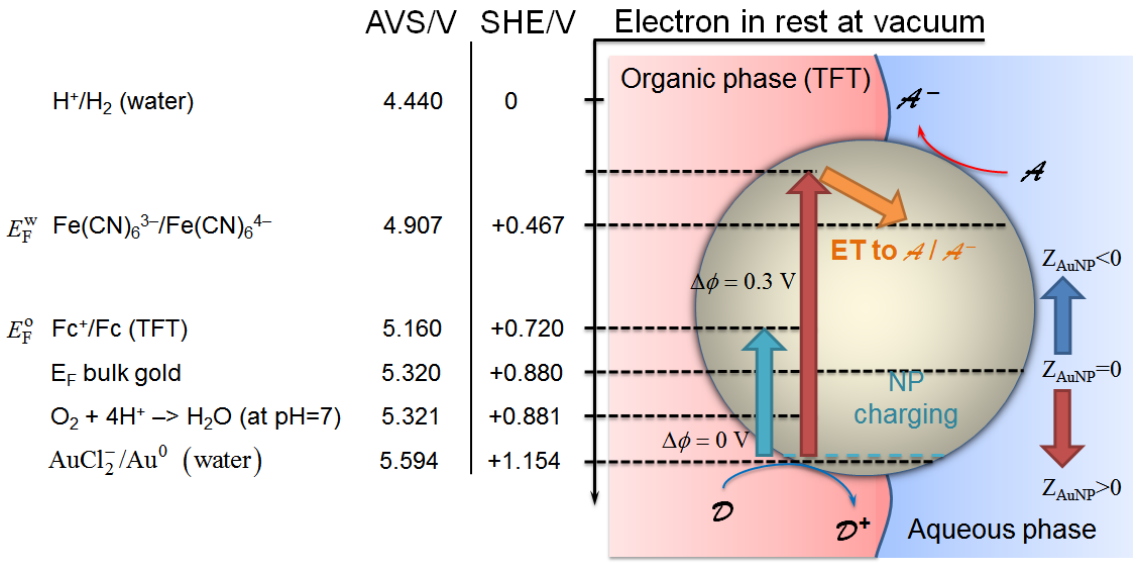

Fig. 3. **Mechanism of interfacial redox electrocatalysis by floating gold nanofilms.** Equilibration of the Fermi level of the electrons in a single AuNP within a gold nanofilm (E_F^{NP}) adsorbed at a liquid-liquid interface with those of two redox couples in solution, a hydrophilic electron acceptor species ($\mathcal{A}$) in the aqueous phase and a hydrophobic electron donor species ($\mathcal{D}$) in the organic phase. The AuNP is charged during this process by $\mathcal{D}$, for example ferrocene (Fc). The AuNP acts as an "interfacial reservoir of electrons", and the final position of E_F^{NP} (a turquoise line for $\Delta_o^w\phi$ = 0 V and a red line for $\Delta_o^w\phi$ = 0.3 V, respectively) is determined by the kinetics of both the oxidation half-reaction on the organic side of the interfacial gold nanofilm and the reduction half-reaction on the aqueous side (for example O_2 reduction). Interfacial electron transfer (IET) between the two redox couples *via* the conductive AuNP, and the provision of a catalytic surface in the specific case of O_2 reduction, significantly enhance the kinetics of IET. The standard redox potentials of all redox couples are expressed *versus* both the Standard Hydrogen Electrode (SHE) and Absolute Vacuum Scale (AVS), respectively, and the organic phase is α,α,α-trifluorotoluene (TFT). Adapted from Ref. [6] with permission from Elsevier, copyright 2015.

Moreover, the AuNPs provide a catalytic surface to further negate the kinetic barriers to IET at bare liquid-liquid interfaces. Additional thermodynamic driving force can then be provided by adjusting $\Delta_o^w\phi$ to establish further control over both the rate of a reaction and the direction of electron transfer across the interface. As a proof-of-concept, interfacial gold nanofilms were shown to effectively catalyse IET between a lipophilic electron donor redox couple, ferrocenium cation/ferrocene, and a hydrophilic electron acceptor redox couple, ferri/ferro-cyanide [7], see

Fig. 4A. The peak-to-peak separation for IET reduced significantly from above 90 mV in the absence of the gold nanofilm (**Fig. 4B**) to between 65 and 70 mV in its presence (**Fig. 4C**). Additionally, a clear shift of the ratio of the forward and reverse peak current towards unity was observed in the presence of the gold nanofilm. Furthermore, dissolved oxygen (O_2) in the aqueous phase can be reduced to H_2O_2 and H_2O by IET from either the lipophilic electron donor redox couple decamethylferrocenium cation/decamethylferrocene [6], as shown in **Fig. 4D-E**,or 1,1'-dimethylferrocenium cation/1,1'-decamethylferrocene [8].

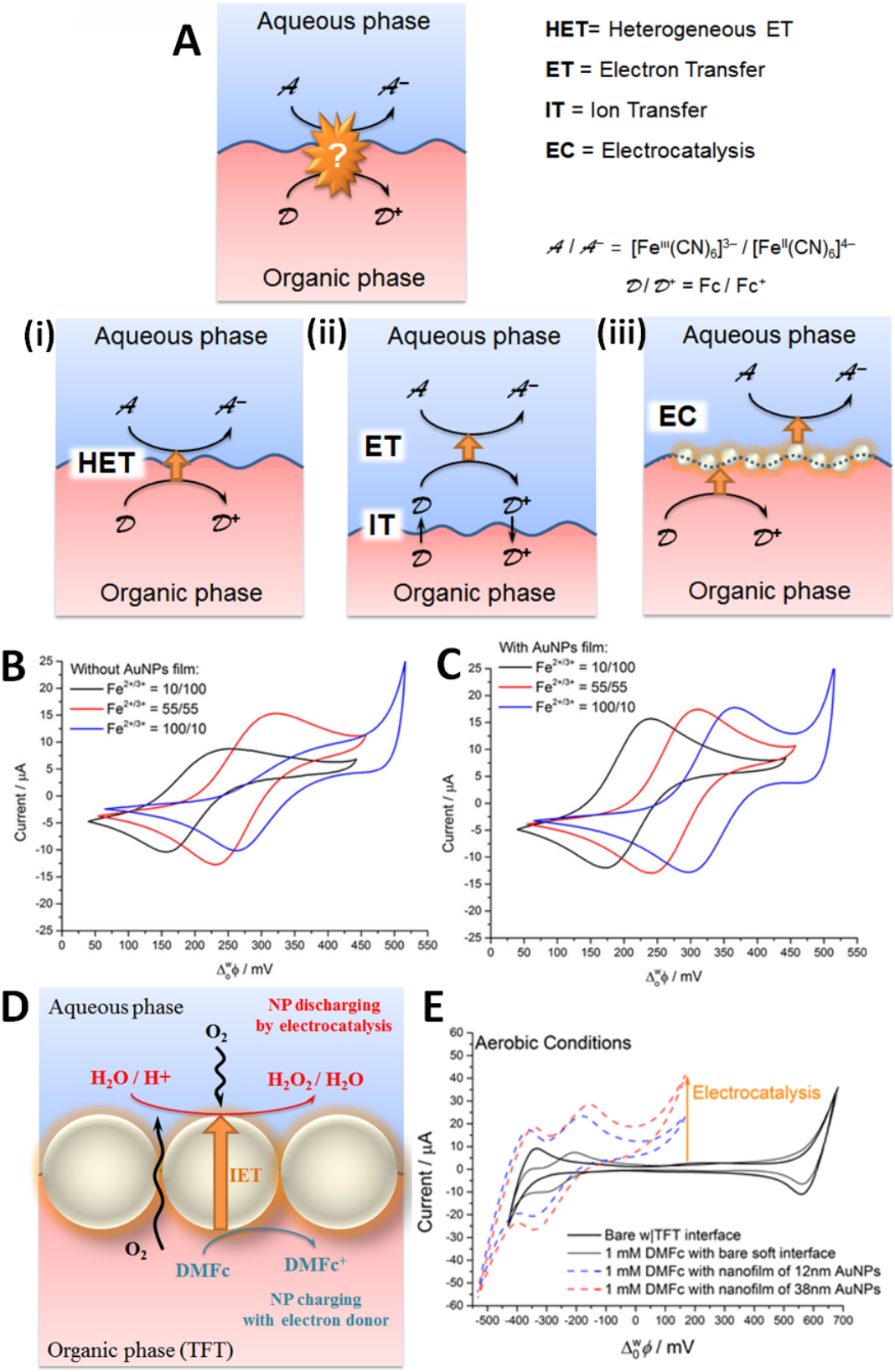
A
Aqueous phase
Organic phase
HET= Heterogeneous ET
ET = Electron Transfer
IT = Ion Transfer
EC = Electrocatalysis
A / A⁻ = [Fe^III(CN)6]3− / [Fe^II(CN)6]4−
D / D+ = Fc / Fc+
(i)
HET
(ii)
ET
IT
(iii)
EC
B
Without AuNPs film:
Fe2+/3+ = 10/100
Fe2+/3+ = 55/55
Fe2+/3+ = 100/10
Current / µA
C
With AuNPs film:
D
NP discharging by electrocatalysis
H2O / H+
H2O2 / H2O
O2
IET
DMFc
DMFc+
NP charging with electron donor
Organic phase (TFT)
E
Aerobic Conditions
Electrocatalysis
Bare w|TFT interface
1 mM DMFc with bare soft interface
1 mM DMFc with nanofilm of 12nm AuNPs
1 mM DMFc with nanofilm of 38nm AuNPs

Fig. 4. Experimental evidence of interfacial redox electrocatalysis by floating gold nanofilms. (**A**) Possible mechanisms, each leading to a measurable current across the ITIES when an electron donor species ($\mathcal{D}$, such as the ferrocenium cation/ferrocene redox couple; Fc^+/Fc) is present in the organic phase and an electron acceptor species ($\mathcal{A}$, such as ferri/ferrocyanide; $[Fe^{III}(CN)_6]^{3-}/[Fe^{II}(CN)_6]^{4-}$) is present in the aqueous phase: (**i**) bimolecular IET, (**ii**) a homogeneous electron transfer-ion transfer (ET-IT) mechanism, and (**iii**) interfacial redox electrocatalysis with the floating gold nanofilm acting as a bipolar electrode. The orange arrow indicates the ET reaction with a rate constant, k^0. Adapted with permission from Ref. [7]. Copyright 2015 American Chemical Society. CVs of ET between the oil solubilised Fc^+/Fc redox couple and the aqueous $[Fe^{III}(CN)_6]^{3-}/[Fe^{II}(CN)_6]^{4-}$ redox couple, with various ratios between Fe^{2+} and Fe^{3+} investigated, both (**B**) in the absence and (**C**) in the presence of an interfacial gold nanofilm. Scan rate for all CVs was 10 mV s^{-1} and the organic phase was TFT. Adapted with permission from Ref. [7]. Copyright 2015 American Chemical Society. (**D**) Mechanism of O_2 reduction in the aqueous phase by charging a floating gold nanofilm with an electron donor (such as decamethylferrocene, DMFc) in the organic phase. The gold nanofilm acts as a barrier-free shortcut for IET to the aqueous phase. Adapted from Ref. [6] with permission from Elsevier, copyright 2015. (**E**) CVs provide clear evidence of IET between DMFc and aqueous O_2 *via* the floating gold nanofilm due to the appearance of a significant current wave at $\Delta_0^{\mathrm{w}}\phi$ = 50 mV under aerobic conditions only. The scan rate was 25 mV s^{-1} in all cases and the organic phase was TFT. Adapted from Ref. [6] with permission from Elsevier, copyright 2015.

3.2 Nanoplasmonics

Localised surface plasmon resonance (LSPR) occurs when the incident light frequency impacting a AuNP is resonant with the collective oscillation of the conduction band electrons [38]. LSPR leads to a marked enhancement in the local (near field) electromagnetic field at the surface of the AuNP in comparison to the incident light. Yang *et al.* have used a three dimensional finite difference time domain (3D-FDTD) method to clarify the LSPR-based optical properties of AuNPs adsorbed at the water–oil interface, including near field distribution and far field absorption [39]. In the case of a AuNP adsorbed at a liquid-liquid interface, the presence of an underlying substrate (*i.e.,* the oil phase) distorts the distribution of the plasmon field around the AuNP (see **Fig. 5(i)-(iv)**). The latter is due to the change of the dielectric function at one side of the AuNP causing the LSPR to be either red- or blue-shifted [3,39–44].

It is important to distinguish that “localised” in LSPR refers to the plasmonic response of separate, non-interacting AuNPs only. This is typically the case for AuNPs dispersed in a colloidal solution or for a hypothetical situation where a single AuNP adsorbs at a liquid-liquid

interface, as modelled by Yang *et al.* in **Fig. 5(i)-(iv)** [39]. However, each AuNP in a gold nanofilm inevitably interacts with its neighbouring AuNPs, and thereby all AuNPs in a gold nanofilm affect each other's plasmonic responses. Thus, herein, firstly we refer to extinction peaks of out-of-plane (transverse) AuNP plasmon oscillations for interacting AuNPs adsorbed at a water-oil interface as simply surface plasmon resonance (SPR) bands. Secondly, in-plane (longitudinal) propagating plasmon oscillations give rise to the appearance of additional "coupling mode" extinction peaks (red-shifted in comparison to those due to SPR, see **Fig. 5B**) that, herein, are referred to as surface plasmon coupling (SPC) bands.

The "hot-spots" formed between plasmonically coupled AuNPs experience hugely enhanced electromagnetic fields. Indeed, Yang *et al.*'s study concluded that the hugely enhanced electromagnetic fields experienced by molecular species in "hot-spots" between adjacent AuNPs in an interfacial gold nanofilm enhances their detection efficiency by Raman scattering in excess of 10^7 –10^9 fold upon excitation with a laser of appropriate wavelength [39]. Such a phenomenon is known as surface-enhanced Raman spectroscopy (SERS) [45], an analytical method capable of providing molecular fingerprint information with ultrahigh surface sensitivity.

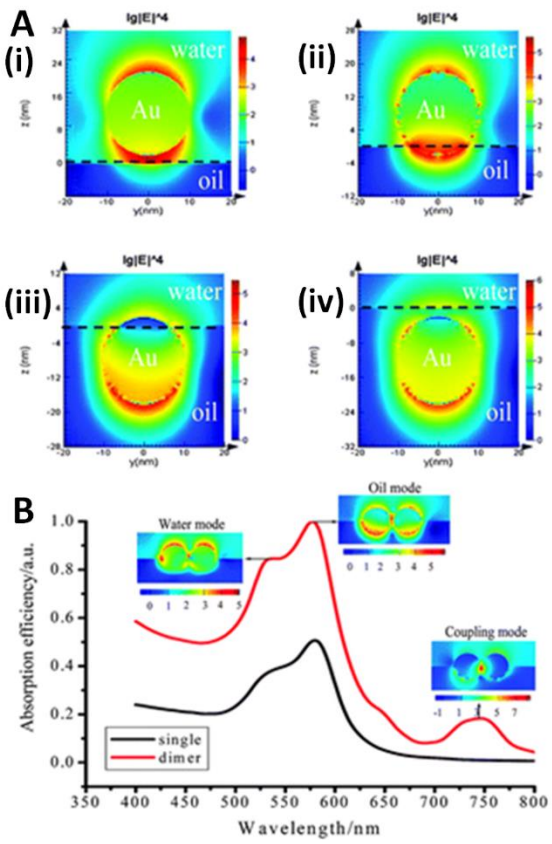

Fig. 5. Distortion of the distribution of the plasmon field around AuNPs floating at a liquid-liquid interface. (**A**) Finite difference time domain (FDTD) calculated SERS electromagnetic enhancement distribution in the yz-plane at the frequency of LSPR for various interfacial positions of a AuNP: (**i**) 2 nm above the interface, (**ii**) 2 nm submerged into the oil, (**iii**) 2 nm remaining in water, and (**iv**) 2 nm below the interface. The dashed line represents the water–oil interface. (**B**) Calculated absorption spectra of AuNP dimers (red line) at the water–oil interface and the corresponding electric field distribution at three SPR peaks (SPR "water mode", SPR "oil mode" and SPC "coupling mode"). Adapted from Ref. [39] with permission from the PCCP Owner Societies.

The SPR and SPC extinction bands observed for AuNPs represent both light absorption and scattering by the AuNPs. Reflection can be considered a special case for light scattered along the specular direction. Furthermore, the AuNPs characteristic SPR wavelengths shift with changes to the medium refractive-index. Thus, as the introduction of analyte molecules influences the bulk refractive index of the AuNPs environment, the resulting shifts in SPR maxima position are the basis of SPR sensors [46]. Both extinction (*i.e.,* transmission expressed in log units) and reflectance measurements have been used to monitor shifts in the SPR maxima

position on introduction of an analyte, with Kedem *et al.* demonstrating that reflectance measurements are more sensitive due to the dominance of absorption in transmission spectroscopy [47].

Thus, using interfacial gold nanofilm sensors, the resulting SERS or SPR-based nanoplasmonic sensors have the potential to facilitate the identification of single molecules attached, or located in close proximity, to the AuNP surface. The defect-free nature of the interface allows the creation of gold nanofilms with an exceptionally homogeneous distribution of "hot-spots", difficult to achieve using either bottom-up or top-down approaches on solid substrates. This key feature maximises the reproducibility of the resulting SERS or SPR-based nanoplasmonic sensors. Prospective floating gold nanofilm based SERS and SPR sensors will be discussed in more in detail in Sections 6 and 7, respectively.

3.3 Optical applications

A series of theoretical studies [48–53] have shown that coupling between localised surface plasmons of AuNPs in an interfacial gold nanofilm leads to significant reflection of light from the interface. The latter is perhaps surprising as only a monolayer of AuNPs is required to achieve this nanoplasmonic mirror-effect. When incident light strikes strongly coupled interfacial AuNPs, light is scattered with phase coherence from AuNP to AuNP (in contrast to non-plasmonically coupled single AuNPs that scatter light in random directions). The result is that the reflection coefficient is very high for an interfacial gold nanofilm, with reflection dominating over transmission, and dependent on the wavelength of incident light. From a practical point-of-view, Smirnov *et al.* [3] have shown that the size of the AuNPs is critical. Small AuNPs (less than 15 nm in diameter) are capable of effectively absorbing incident light, whereas larger AuNPs (above 25-30 nm) are more suited for liquid mirrors applications due to efficient reflection of light (in agreement with theory) [3]. The larger AuNPs absorb very little light due to being low dissipation materials that facilitate long-lived plasmons [49]. By comparison, NPs of aluminum, for example, would absorb significant amounts of light at the interface *via* dissipation of surface plasmons [49]. Thus, the reversible electrovariable movement of AuNPs both "on and off" the interface and laterally as a function of $\Delta_0^{\mathrm{w}}\phi$ lays the foundations for a host of potential technological applications of interfacial gold nanofilms in the realm of optics.

3.4 Plasmonic photocatalysis

Finally, the topic of plasmon-enhanced photo-reactions with floating gold nanofilms is not explored in detail in this perspective. However, it is worth mentioning briefly as conflicting reports have emerged regarding whether photocurrents at porphyrin-sensitised liquid-liquid interfaces can be significantly enhanced by devising protocols that incorporate plasmonic metallic NPs into the photoactive interfacial films [4,54,55]. Insights from such studies may potentially find applications in future artificial photosynthesis systems [56,57]. The underlying fundamental reasons for any enhanced photocurrents are as yet unresolved with electrocatalytic and/or plasmonic factors needing to be considered. Nagatani *et al.* [55] and Schaming *et al.* [54] observed increased photocurrents that may be attributed to increased absorption due to surface plasmons and light-trapping effects, improved charge separation due to a localised intense electromagnetic field, or perhaps electron storage effects that alter the Fermi level of the interfacial gold nanofilm. Alternatively, the photocurrents may actually decrease, as observed by Gschwend *et al.* [4], as the surface area of the liquid-liquid interface becomes "blocked" with AuNPs, reducing the interfacial concentration of excited porphyrin molecules. Thus, some key questions remain unresolved. Which of the noted possible factors dominate the enhanced photo-responses seen by Nagatani *et al.* and Schaming *et al.*? Do the observations of Gschwend *et al.* negate all of the possible beneficial electrocatalytic or plasmonic attributes of the interfacial AuNPs? Each of the three studies to date introduced AuNPs to the electrochemical cell using very different experimental protocols, and therein likely lays the discrepancies between these preliminary studies.

4. Experimental strategies to functionalise liquid-liquid interfaces with floating gold nanofilms

In this section, we discuss experimental strategies to induce the adsorption of pre-formed colloidal spherical AuNPs at liquid-liquid interfaces. A comprehensive review of the adsorption of other nanomaterials at liquid-liquid interfaces (beyond the scope of this review), including both non-spherical nanomaterials, *e.g.,* 1D nanorods or 2D sheets, and Janus NPs was recently provided by Booth and Dryfe [58]. Additionally, the electrodeposition of AuNPs at the ITIES has

been reviewed by Dryfe *et al.* [59]. The latter approach "decorates" the ITIES with AuNPs, though not to the extent that gold nanofilms of densely packed assemblies of uniformly arranged AuNPs are formed.

4.1. Thermodynamics of nanoparticles at the liquid-liquid interface

Several key studies have outlined in detail the various forces at play that dictate the adsorption of NPs at a liquid-liquid interface [60–65]. In this regard, Flatté *et al.* [65] provided a particularly useful numerical model consisting of analytical equations that describe several key contributions to the total free energy of the biphasic system upon adsorption of NPs at the liquid-liquid interface. The key energies identified were (i) the energy of capillary forces, (ii) the energy devoted to changing the solvation sphere as the NP moves from an aqueous to organic environment, (iii) the line tension and (iv) the presence of an external electric field (applicable only for NPs adsorbed at an ITIES). Recently, Smirnov *et al.* [26] created a very assessable calculator using Flatté *et al.*'s equations (available online in the supporting information of their article). The calculator describes the balance of the interfacial energies at a non-polarised liquid-liquid interface for NP adsorption as a function of NP size, dielectric constant of the organic solvent, surface charge of the NP, and three-phase contact angle of the NP (θ_0).

The main driving force entrapping a NP at a liquid-liquid interface is the capillary energy, *i.e.,* the energy a system gains if a NP occupies a portion of the interface. Primarily, the capillary energy is dictated by the interfacial surface tension ($\gamma_{w/o}$) and θ_0 (see **Fig. 6A** for a graphical representation of the precise meaning of θ_0). On the other hand, the solvation energy acts as a barrier to NP adsorption. As a charged NP transfers from a more polar to less polar medium (so from water to oil), the contribution of the solvation energy to the overall energetic balance increases significantly, especially once the NP pierces the organic side of the interface. The line tension contains all kinds of interactions pushing NPs away from the interface; whereas an external electric field at an ITIES can be applied to forcibly entrap NPs at the interface (discussed *vide infra*).

A typical energetic profile of NP adsorption at a water-DCE interface is demonstrated in **Fig. 6B(i)**. On the aqueous side of the interface, approach of the NPs to the liquid-liquid interface is

impeded by an energy barrier. As the NPs cannot reach the potential well that exists at the interface, no interfacial assembly of adsorbed NPs takes place. However, if $\gamma_{w/o}$ or θ_0 are tuned (for example by changing the organic solvent from DCE to propylene carbonate as shown in **Fig. 6B(ii)**), adsorption of NPs is facilitated. The latter is possible as the barrier on the aqueous side of the interface has lowered, increasing the likelihood of the NPs falling into the potential well at the interface and becoming trapped [3,26,66].

Once two or more AuNPs assemble at the liquid-liquid interface Coulombic repulsive and van der Walls attractive forces exert influence on the adsorbed AuNPs. Thus, the surface charge density (σ) of adsorbed AuNPs critically influences their tendency to adsorb and their equilibrium interfacial surface coverage [60,62–64]. In the case of large particles (typically larger than 1μm), their weight and associated additional capillary forces need to be considered (not discussed herein).

Thus, all-in-all, three main strategies have been developed to induce AuNP adsorption at the interface by reducing the total free energy of the biphasic system either by manipulating: (i) electrostatics (*i.e.,* minimising Coulombic repulsion between interfacially adsorbed AuNPs by reducing screening effects, decreasing σ, or applying an electric field at the ITIES), (ii) hydrophobicities of adsorbed AuNPs (*i.e.,* affecting $\gamma_{NP/w}$, $\gamma_{NP/o}$ and θ_0, see **Fig. 6A**), or (iii) interfacial surface tension (*i.e,* decreasing $\gamma_{w/o}$). Also, simultaneously achieving a synergistic mix of more than one effect is common (*e.g.,* decreasing σ and bringing θ_0 closer to 90° with one strategy). Finally, as the adsorption of AuNPs is typically a kinetically controlled process dictated by the AuNP's Brownian motion [67], many of the strategies discussed involve emulsification or vigorous shaking of the biphasic systems to accelerate AuNP adsorption.

4.2. Experimental strategies

Bell and co-workers [67–69] have classified a series of chemically diverse molecules (*e.g.,* tetrabutylammonium nitrate and 4-tertbutylcalix[4]arene tetraethylester (Na^+) complex) that when introduced to a biphasic system act as electrostatic "promotors" of AuNP adsorption. A promotor must (i) contain a hydrophobic ion of opposite charge to the AuNP, (ii) not directly adsorb onto the AuNP (*i.e.,* displace the original stabilising ligand) and (iii) induce adsorption

when present at low concentrations. Promoters induce adsorption by condensation of the hydrophobic ions on the organic side of the interface, thereby screening Coulombic repulsion acting on the portions of each AuNP submerged into the organic solvent [67–69], as shown in **Fig. 6C(i)**. The latter combined with the attractive van der Walls forces determines the interparticle separation distances at the interface. Both hydrophilic salts present at low (ppm) concentrations and amphiphilic salts with hydrophobic ions of identical charge to the AuNP reduce Coulombic repulsion only in the aqueous phase. Thus, neither can act as promoters. Nevertheless, Turek *et al.* demonstrated that by increasing the ionic strength in the aqueous phase by addition of salt, the reduction in Debye length at the surface of each AuNP can be sufficient to induce adsorption upon centrifugation [70].

A variety of methods have been introduced to reduce σ. Modification of AuNPs with stabilising ligands that terminate in carboxylic groups (*e.g.,* 3-mercaptopropionic acid, 4-mercaptobenzoic acid, 16-mercaptohexadecanoic acid) allow effective modulation of σ by pH [63,71]. Indeed, such a tactic can be used to reversibly adsorb/desorb AuNPs <10 nm in size from the interface [71]. Another approach is to introduce "modifiers" to the biphasic system. As defined by Bell and co-workers [67,69], a modifier can tune σ, but also synergistically modify the surface hydrophobicity of the AuNPs (*i.e.,* affecting θ_0). Unlike promoters, modifiers may coordinate with the initial ligand on the AuNP or substitute the ligand completely *in situ*, see **Fig. 6C(iii)**. Examples of modifiers include 1-dodecanethiol [72,73], mercaptosuccinic acid in combination with tetraoctylammonium bromide [74], 2,2'-dithiobis[1-(2-bromo-2-methyl-propionyloxy)ethane] (DTBE) [61], poly-N-isopropylacrylamide (PNIPAM) [75] and tetrathiafulvalene [66].

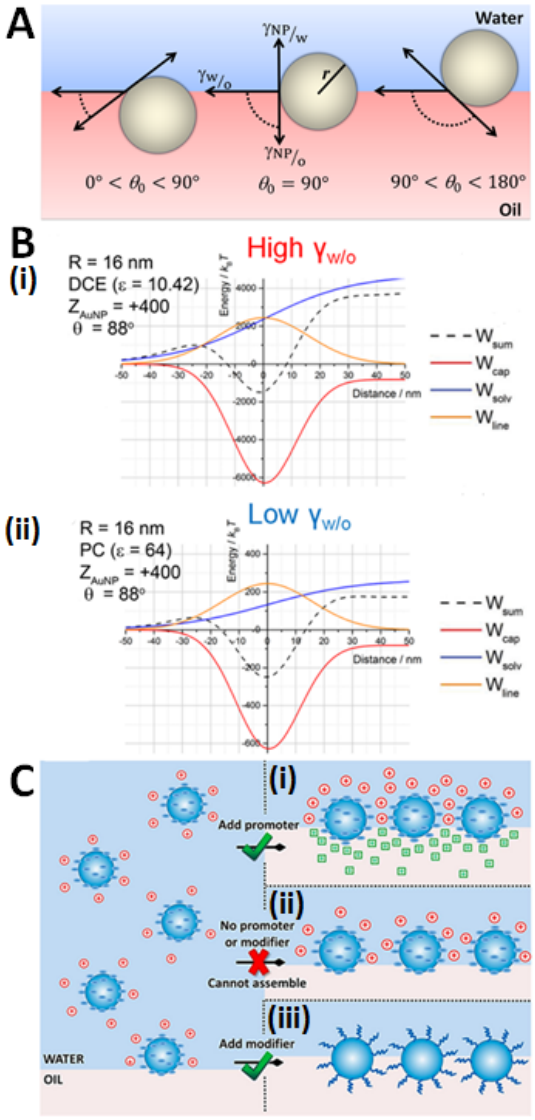

Fig. 6. (**A**) Schematic representation of the position of a AuNP at a liquid-liquid interface for a three-phase contact angle (θ_0) with the interface less than 90° (left), equal to 90° (center), and larger than 90° (right). θ_0 is defined as the angle between the water-oil interface and the NP-oil side of the tangent plane at the line of contact. $\gamma_{NP/w}$, $\gamma_{NP/o}$ and $\gamma_{w/o}$ are the interfacial energies of the NP-aqueous phase interface, NP-organic solvent interface, and water-organic solvent interface, respectively. The effective radius of the AuNP is *r*. **(B)** Contribution of the components of capillary forces (W_{cap}, red line), solvation energy (W_{solv}, blue line) and line tension (W_{line}, orange line) to the overall energy profile (W_{sum}, dashed black line) for a AuNP adsorbed at (**i**) a water-1,2-dichloroethane (DCE) interface ($\gamma_{w/o}$ ~ 30 mN/m) and (**ii**) a water-propylene carbonate (PC) interface ($\gamma_{w/o}$ ~ 3mN/m). The excess of charge on the AuNP (Z_{AuNP}) was set to +400 and θ_0 was set to 88°. These calculations were carried out using Mathematica software and the CDF file is available in the supplementary information of Ref. [26]. Adapted from Ref. [26] with permission from The Royal Society of Chemistry. (**C**) On contact between an

aqueous colloidal solution of AuNPs and an immiscible oil phase, a few AuNPs are driven to the interface by the reduction of interfacial energy. However, the strong potential barrier on the aqueous side of the interface (seen at a distance of ~20 nm from the interface for the experimental conditions modelled with the dashed line for W_{sum} in (**B**)(**i**)) keeps most AuNPs dispersed in the aqueous phase. Thus, as shown in **C**(**ii**), self-assembly of the AuNPs into a gold nanofilm under these conditions is not possible. On the contrary, the addition of promoters **C**(**i**) or modifiers **C**(**iii**) significantly reduce this potential barrier by providing charge screening, changing the AuNPs' surface charge density (σ), or synergistically modifying the AuNPs hydrophobicity (*i.e.,* affecting θ_0). Adapted with permission from Ref. [67]. Copyright 2016 American Chemical Society.

Arguably, the most widely used method of inducing interfacial AuNP adsorption is to introduce an alcohol, such as ethanol or methanol, to the biphasic system that simultaneously reduces σ and $\gamma_{w/o}$, ultimately allowing θ_0 to approach the optimal 90° [3,4,6,7,54,60,61,63,72,73,76–79]. Alcohols may firstly reduce σ by competitive displacement of citrate ligands (*i.e.,* acting as modifiers) [60,63]. Additionally, water miscible alcohols will lower the dielectric constant of the aqueous phase as a function of alcohol content, thereby gradually decreasing σ [73]. Experimental evidence [80] and molecular dynamic (MD) simulations [81] indicate that the presence of a mutually miscible alcohol across both phases reduces $\gamma_{w/o}$. Indeed, gold nanofilms have also been successfully formed at pure aqueous-pentanol interfaces [82]. Finally, the ITIES was modified using a minimum amount of methanol by initially suspending the citrate-stabilised AuNPs in a methanol solution, and then injecting this alcoholic colloidal solution directly at the ITIES using a micro-syringe [4,6,7,83], see **Fig. 7**. Such an approach was beneficial to prevent artifacts in ensuing electrochemical studies.

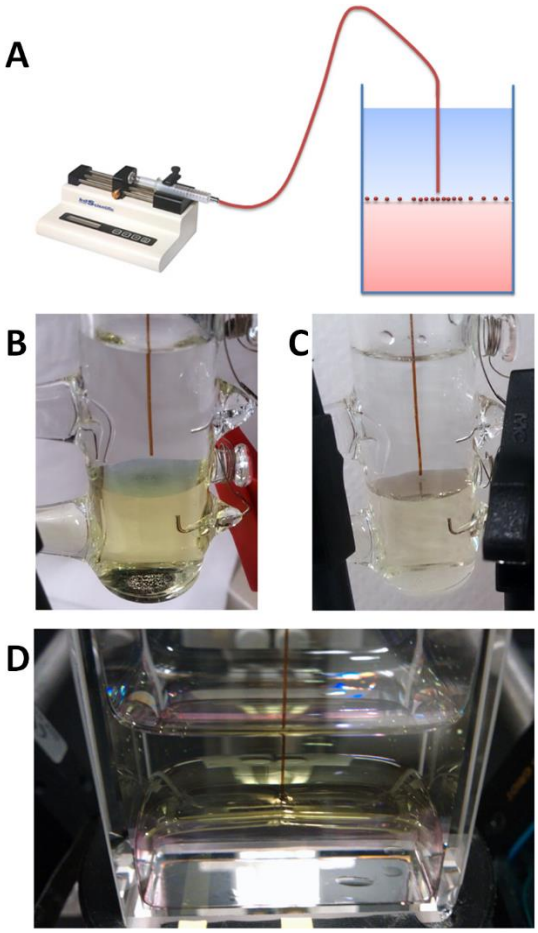

Fig. 7. Functionalisation of liquid-liquid interfaces with floating gold nanofilms by precise injection of AuNPs suspended in methanol at the interface. (**A**) Schematic of the capillary and syringe-pump setup used to settle AuNPs directly at the ITIES allowing precise control over the AuNP surface coverage. Examples of gold nanofilms prepared at flat water-trifluorotoluene interfaces in 4-electrode electrochemical cells using AuNPs with mean diameters of (**B**) 12 nm and (**C**) 38 nm. Flat liquid-liquid interfaces were achieved by partial silanisation of the bottom half of the electrochemical cell glass walls. (**D**) Gold nanofilms were also prepared on larger curved soft interfaces using a 2 x 4 cm quartz cell. Adapted with permission from Ref. [7]. Copyright 2015 American Chemical Society.

Intensive mixing of immiscible biphasic systems of extremely low $\gamma_{w/o}$, such as the aqueous-propylene carbonate system ($\gamma_{w/o}$ = *ca.* 3 mN·m^{-1}), can directly lead to gold nanofilm formation [83]. The disadvantage of using propylene carbonate, however, is its inability to form an electrified ITIES with a wide PPW; thereby, limiting its potential utility.

4.3. Electrovariable nanofilms

Uniquely, an ITIES provides the additional ability to externally tune the electric field felt by AuNPs in close proximity to the interface. Thus, for negatively charged colloidal AuNPs in the aqueous phase, polarisation of the ITIES negatively (*i.e.,* the aqueous phase is negatively charged with respect to the organic phase) will push the AuNPs towards the interface and potentially induce gold nanofilm formation (see **Fig. 8, left panel**). On the contrary, positive polarisation will repel the AuNPs from the interface, electrostatically dragging them back into the bulk aqueous phase and disassembling any gold nanofilm formed (see **Fig. 8, right panel**).

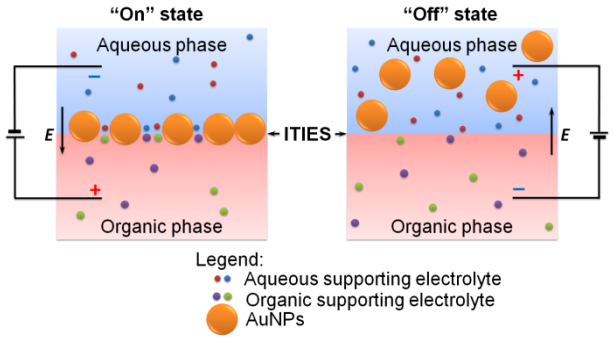

Fig. 8. Electrovariable gold nanofilm formation by polarisation of the ITIES. (**Left panel**) On application of a negative potential at the ITIES the negatively charged AuNPs are electrostatically "pushed" to the ITIES and form a gold nanofilm. (**Right panel**) On application of a positive potential at the ITIES the AuNPs are electrostatically "repelled" from the ITIES and the gold nanofilm disassembles.

The voltage-induced reversible adsorption and desorption of NPs is dependent on their size and σ, and has been demonstrated for AuNPs < 2 nm in size [5,84] and core-shell gold-silver NPs ca. 16 - 20 nm in size (but with a 4-fold increase in σ in comparison to pure AuNPs) [85]. However, AuNPs < 2 nm in size do not form lustrous gold nanofilms. To date, the precise experimental conditions to reversibly absorb/desorb more technologically relevant gold nanofilms composed of larger AuNPs within the range of $\Delta_0^{\mathrm{w}}\phi$ applicable at the ITIES have not been identified. However, lateral movement of larger AuNPs on the fluidic interface may be much more accessible. Bera *et al.* showed that the interparticle distance of interfacial adsorbed 2 nm

AuNPs can be varied by as much as 1 nm by tuning $\Delta_{o}^{w}\phi$ [5]. Gschwend *et al.* demonstrated that changes in $\gamma_{w/o}$ in the presence of a surfactant as a function of $\Delta_{o}^{w}\phi$ can induce rapid lateral movement of relatively large 12 nm AuNPs from one position on the ITIES to another, thereby behaving as "electrovariable Marangoni shutters" (discussed in Section 7) [4].

5. The critical influences of interfacial AuNP immersion depth and interparticle spacing for redox electrocatalysis, nanoplasmonic sensors and electrovariable optics applications

5.1. Redox electrocatalysis

The immersion depth at the interface (*i.e.,* θ_0 values) may influence a AuNPs catalytic activity as an interfacial bipolar electrode by altering the ratio of surface area available for electron transfer reactions between the water and organic sides of the interface [7]. Additionally, the potential drop across the ITIES is not uniformly spread between the aqueous and organic back-to-back diffuse layers. Thus, the rate of electrochemical reactions taking place on the aqueous side of the interface may benefit from a greater proportion of the potential drop taking place there.

Charge transport along a gold nanofilm is achieved by multiple electron tunneling events (*i.e.,* electrons hopping between conductive AuNPs separated by a dielectric medium). The tunneling probability falls off exponentially with distance [86]. The latter was demonstrated by Wuelfing *et al.* [87] who observed an exponential decay of conductivity as a function of the thickness of an alkanethiol matrix separating gold monolayer protected cluster (MPC) cores cast onto interdigitated array electrodes (**Fig. 9A**). The MPC core separation distances in the film were easily varied by choice of the alkanethiol monolayer chain length [87]. Thus, the extreme sensitivity of the tunneling probability to MPC core separation distances clearly highlights the need to precisely tune interparticle spacing to achieve truly conductive interfacial gold nanofilms. The latter would permit a massively increased cross-sectional area of reaction to facilitate IET by providing a continuous conductive interfacial route for electrons to travel from donor to acceptor molecules on either side of the interface. Thus, electrons injected anywhere on the gold nanofilm can be discharged at any point of contact on the opposite side of the

interface. Support for the latter mechanism is evident from the significant increases in the rates of reaction for biphasic H_2 evolution and O_2 reduction due to redox electrocatalysis by interfacially adsorbed conductive bare or catalytic NP decorated carbon materials (*e.g.,* graphene or CNTs) [88–93]. The mechanism of redox electrocatalysis for these conductive carbon materials is explained in detail in a recent review [32], and incorporates most of the elements of redox electrocatalysis by gold nanofilms described in Section 3.

5.2. Nanoplasmonics and optics

Critically, for the performance of interfacial gold nanofilms as nanoplasmonic sensors, the strength of plasmon coupling, and associated "hot-spots" for SERS sensing, is dependent on the distance between the AuNPs [38]. Furthermore, Jain *et al.* [94,95] demonstrated that as the interparticle gap decreases, the strengthening electric field causes a near-exponential increase in the sensitivity of the SPR frequency shift to the medium refractive-index (**Fig. 9B & C**).

Finally, with regard to electrovariable optics, theoretical [48–53] and experimental [79,96] studies have indicated that resonant light reflection, allowing gold nanofilms to act as nanoplasmonic mirrors, depends on the material of the NPs, their size and interfacial surface coverage (*i.e.,* average interparticle spacing should be substantially less than half the AuNP size [2]). Unfortunately, key factors that are beneficial for reflective interfacial gold mirror formation are diametrically opposed to facilitate electrovariable "on/off" behaviour. On the one hand, the AuNPs must be > 25 nm in size and suitably functionalised to have as low a σ as possible in order to achieve very dense packing at the interface. On the other hand, such large AuNPs are typically irreversibly trapped in a potential well at the liquid-liquid interface upon adsorption (considered in Section 4). An obvious approach is to increase σ causing an increase in the electrostatic driving force for desorption to overcome the trapping potential well. However, an increase in σ will also likely negate the formation of a dense gold nanofilm in the first instance. Thus, imaginative approaches to find the correct balance of these opposing factors are required to achieve "on/off" electrovariable optics. Future approaches will investigate the choice of AuNP stabilising ligand and the modification of the properties of the liquid-liquid interface itself by introduction of surfactants or use of mixed solvents.

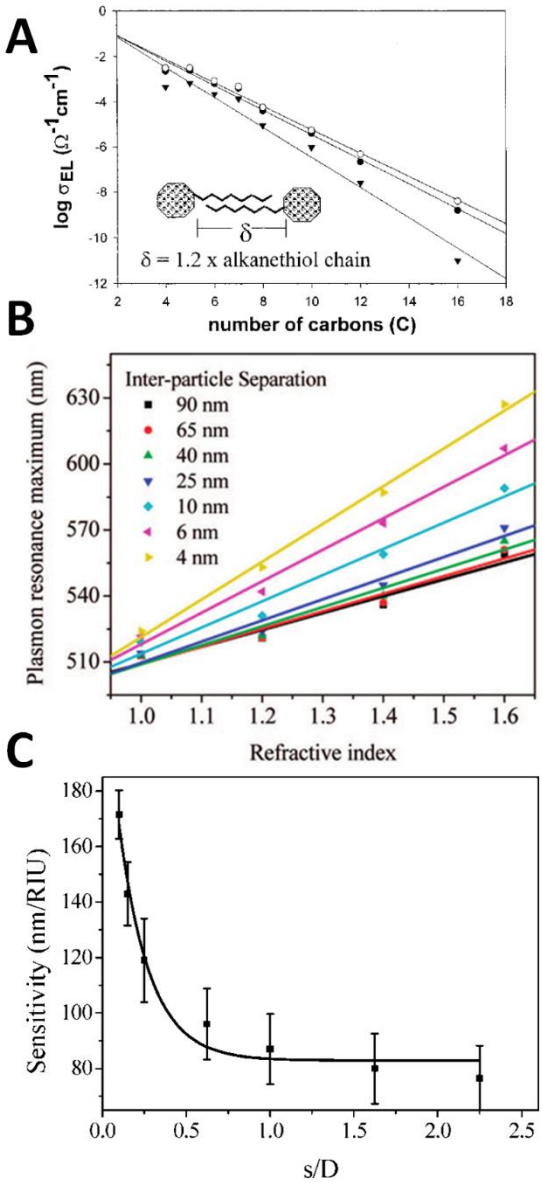

Fig. 9. (**A**) The conductivity of gold monolayer protected cluster (MPC, specifically of $Au_{309}(Cn)_{92}$) solid state films cast onto an interdigitated electrode surface decays exponentially as a function of the numbers of carbons in the alkanethiolate chain. The temperature of the measurements was either 70 (solid circle), 30 (hollow circle) or 60 (inverted solid triangle) °C. The inset is a schematic describing the interdigitation of monolayer chains in the solid-state MPC films. Adapted with permission from Ref. [87]. Copyright 2000 American Chemical Society. (**B**) The LSPR maximum of a NP dimer (for polarisation along dimer axis) increases linearly with increasing refractive-index, similar to an isolated NP. However the increase has a much higher slope for dimers with a smaller inter-NP gap. Adapted with permission from Ref. [94]. Copyright 2008 American Chemical Society.(**C**) A plot of the SPR sensitivity (*i.e.,* the slopes of the data

plotted in (B)) *versus* the inter-NP gap (s, normalised by the NP diameter, D) clearly highlights that the SPR sensitivity to the medium increases almost exponentially with decreasing interparticle gap. Adapted with permission from Ref. [94]. Copyright 2008 American Chemical Society.

6. Experimental techniques to characterise floating gold nanofilms

6.1. Surface tension, capacitance and optical techniques

Techniques that monitor the adsorption of AuNPs *in situ* are extremely useful, in particular when multiplexed with a 4-electrode electrochemical cell to track adsorption as a function of applied $\Delta_o^w\phi$. The voltage-induced reversible adsorption and desorption of AuNPs < 2 nm in size, noted earlier, was monitored by *quasi-elastic light scattering (QELS)* [5,84], see **Fig. 10A(i)** for a scheme of the experimental setup. QELS monitors the frequencies of capillary waves of a selected wavelength at the liquid-liquid interface spontaneously generated by thermal fluctuations. The resulting plots of $\gamma_{w/o}$ *vs.* $\Delta_o^w\phi$ are known as electrocapillary curves (**Fig. 10A(ii)**). In the presence of AuNPs the shape of an electrocapillary curve changes significantly, as shown in **Fig. 10A(ii)**, reflecting changes in the number density of AuNPs at the interface.

An alternative experimental approach to measure electrocapillary curves is *pendant drop tensiometry* [97–99]. This technique has yet to be applied to monitor the adsorption of AuNPs as a function of $\Delta_o^w\phi$. Nevertheless, measurements of $\gamma_{w/o}$ for non-polarised water-decane interfaces in the presence of various adsorbed AuNPs clearly highlight the techniques suitability for future studies [100–102].

Electrochemical capacitance measurements at the ITIES have highlighted an increased capacitance at negative potentials in the presence of either citrate-stabilised 16 nm AuNPs [77] or mercaptosuccinic acid-stabilised < 2nm AuNPs [84]. Due to their negatively charged stabilising ligands, the AuNPs are induced to adsorb at a negatively polarised ITIES and excess charge density builds at the interfacial boundary. Additionally, excess charge density may be attributable to interfacial corrugation in the presence of adsorbed AuNPs. Marinsecu *et al.* [103] developed a theoretical model to facilitate further development of such capacitance based characterisation of interfacial AuNP adsorption as a function of $\Delta_o^w\phi$, with experimental

data closely matching the theory (**Fig. 10B**). The non-linear optical technique *surface second harmonic generation (SSHG)* is a powerful surface specific technique that may be applied to the study of molecular species or solid nanomaterials adsorbed at the liquid-liquid interface [104], see **Fig. 10C** for a scheme of the experimental setup. SSHG is ideal for monitoring voltage-induced reversible adsorption and desorption, as exemplified for core-shell gold-silver NPs ca. 16 - 20 nm in size (**Fig. 10D**) [85]. The surface specificity of SSHG arises from the vanishing of the second-order nonlinear susceptibility in centrosymmetric media within the electric dipole approximation [105].

6.2. Physical position and three-phase contact angle of the nanoparticles

In order to understand the measured conductive, catalytic or plasmonic activity of a gold nanofilm, the physical positions of individual AuNPs within the nanofilm need to be determined with nanometer accuracy in terms of interparticle spacing and θ_0 values. The characterisation of AuNPs on solid supports is dominated by electron and scanning probe microscopy techniques (*i.e.,* scanning/transmission electron microscopy (SEM/TEM), and scanning probe microscopy (SPM) such as atomic force microscopy (AFM) and scanning tunneling microscopy (STM)). However, the motion of AuNPs on a fluidic interface makes such *in situ* analysis at liquid-liquid interfaces exceptionally difficult. *Ex situ* analysis, for example by SEM/TEM, *via* transferring the gold nanofilms to solid supports may cause alteration of the initial microstructure, lead to the formation of drying artefacts and, finally, to incorrect interpretation of the obtained data.

Recent reviews have provided an overview of common techniques applied to determine θ_0 values of various nanomaterials at fluidic interfaces [106,107]. Techniques such as capillary rise methods, surface-pressure isotherms or drop shape analysis measure macroscale interfacial properties related to θ_0 through theory, and therefore are indirect. The drawback of such techniques are an inability to analyse the distribution of θ_0 values, with a single average θ_0 value provided and a reliance on assumptions that tend to break down at the nanoscale.

One promising technique designed to overcome these issues *is freeze-fracture shadow casting (FreSCa) cryo-SEM* [108,109]. This technique was used to image ca. 100 nm AuNPs *in situ* at

water-decane interfaces and additionally determine θ_0 values. As the name suggests, the AuNP functionalised liquid-liquid interface is frozen in a liquid propane jet with a speed of up to 10^6 K s^{-1}, then cracked open and imaged. The key is that the interface acts as a weak fracture plane that is preferentially exposed on fracturing, see **Fig. 10E**. Techniques that trap AuNPs in gels, followed by analysis with SEM or AFM, have also been developed [110]. However, potential drawbacks of both FreSCa cryo-SEM and gel-trapping techniques are the deformation of the interface due to the freezing/gelling process and difficulties providing statistically significant individual data points to evaluate the distribution of θ_0 values at the interface.

Costa *et al.* successfully imaged SiO_2 NP monolayers self-assembled at a water-heptane interface with an unprecedented lateral resolution of <10 nm using *amplitude-modulation AFM* [111], see **Fig. 10F** for a scheme of the experimental setup. The development of such real-space *in situ* imaging techniques will allow in-plane structural information, such as the interparticle spacing, to be gathered on a localised area of the interface. This is in sharp contrast to reciprocal techniques, such as X-ray reflectivity (discussed *vide infra*), where structural information is averaged over the finite size of the radiation beam and non-periodic isolated AuNP aggregates or defects in the nanofilm may not be easily detected.

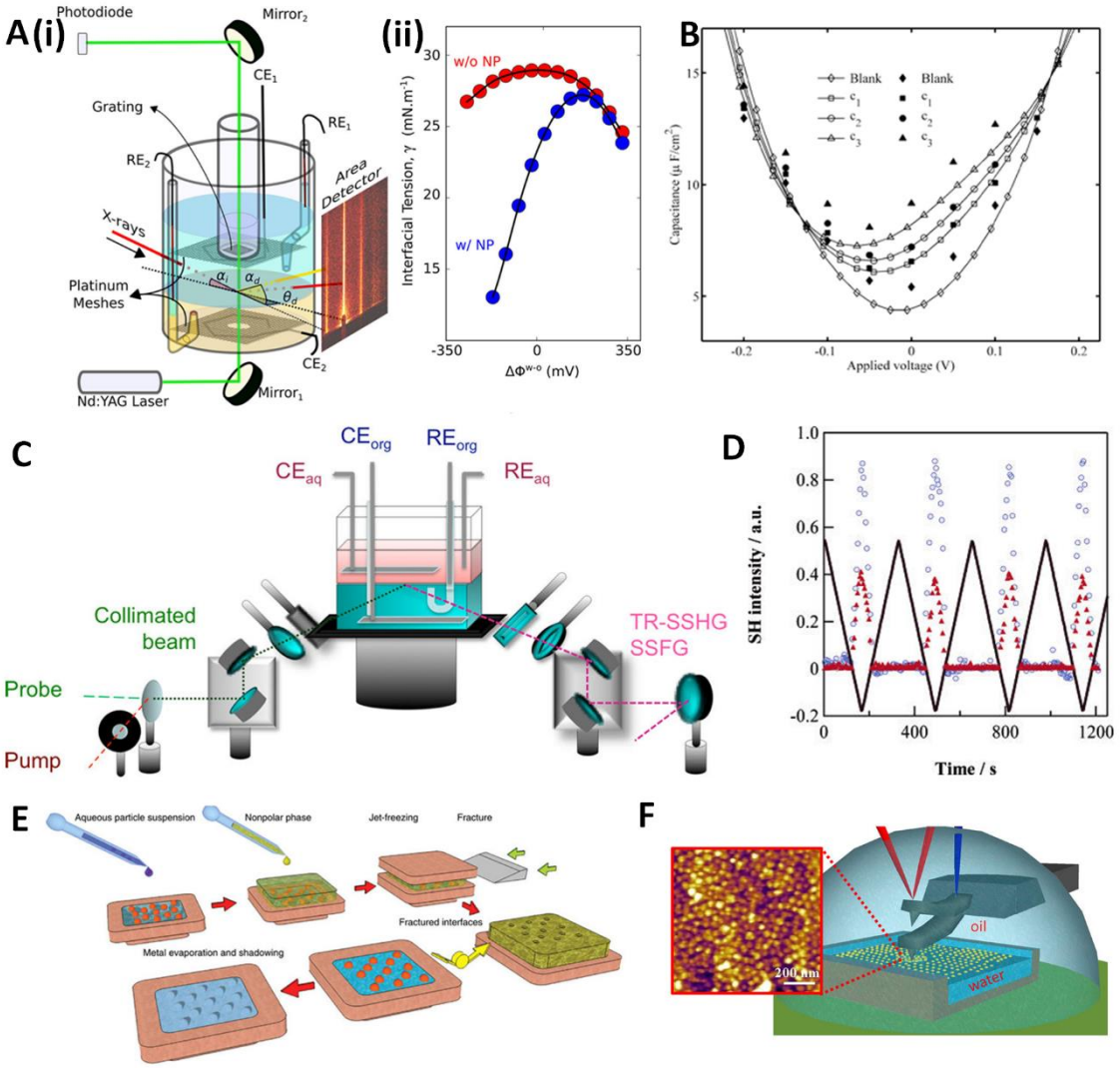

Fig. 10. (**A**) (**i**) is a schematic of a 4-electrode electrochemical cell configured for either *X-ray surface scattering measurements* or *quasi-elastic light scattering (QELS)* interfacial tension measurements (CE_1 and CE_2 are counter electrodes made of Pt mesh; RE_1 and RE_2 are Ag/AgCl reference electrodes). (**ii**) Electrocapillary curve generated using QELS; *i.e.,* a plot of interfacial tension measurements of the water-oil interface as a function of the Galvani potential difference ($\Delta_o^w\phi$) with AuNPs (blue) and without AuNPs (red). Adapted with permission from Ref. [5]. Copyright 2014 American Chemical Society. (**B**) Calculated *specific capacitance curves* (lines) are compared to the data measured (symbols; from Ref. [77]) for various concentrations of AuNPs in the bulk aqueous electrolyte: c_1=0.42 nM, c_2=0.67 nM, c_3=1.26 nM. "Blank" refers to the unpopulated interface. Adapted from Ref. [103] with permission from the PCCP Owner Societies. (**C**) Schematic of the electrochemical *Time-Resolved Surface Second Harmonic Generation (TR-SSHG)* experimental setup (CE = counter electrode, RE = reference electrode, Aq = aqueous phase, and Org = organic phase). Adapted with permission from Ref. [104]. Copyright 2014 American Chemical Society. (**D**) SSHG intensity (symbols) and Galvani potential difference (solid black line) as a function of time at the water-DCE interface for (triangles) $Au_{0.9}Ag_{0.1}$ NPs

and (circles) $Au_{0.6}$ $Ag_{0.4}$ NPs. Adapted with permission from Ref. [85]. Copyright 2007 American Chemical Society. (**E**) Schematics of the sample preparation for *freeze-fracture shadow casting (FreSCa) cryo-SEM* imaging. Reprinted by permission from Macmillan Publishers Ltd: Nature Communications, Ref. [109], copyright 2011. (**F**) Operational scheme of *amplitude-modulation AFM* at a water-heptane interface and images of the NP monolayers. The depth of the water layer confined by a mica container is kept lower than 100 µm and the cantilever is excited by photothermal actuation (blue laser) inside the heptane drop. Adapted with permission from Ref. [111]. Copyright 2016 American Chemical Society.

6.3. X-ray reflectivity and scattering

Several techniques based on scattering of X-rays from liquid-liquid interfaces are capable of determining *in situ* both in-plane and out-of-plane structural information on floating gold nanofilms [5,96,112,113].

X-ray reflectivity measurements identify variations in electron density perpendicular to the liquid-liquid interface [114,115], the experimental setup is identical to that for QELS as shown in **Fig. 10A(i)**. Schlossmann and co-workers showed that the resulting electron density profiles allow the precise interfacial location of a monolayer of 2 nm AuNPs to be determined with sub-nanometer resolution as a function of $\Delta_o^w \phi$ [5]. Under experimental conditions that induce very dense arrangements of AuNPs at the liquid-liquid interface, for example upon lateral compression [112], X-ray reflectivity measurements provide evidence for the formation of interfacial bi- or tri-layers of AuNPs.

Grazing-incidence small angle x-ray scattering (GISAXS) reveals the 2D ordering of the AuNPs within the gold nanofilm, for example changes in the lattice spacing or interparticle separation distance as a function of $\Delta_o^w \phi$ [5] or solution ionic strength [96] have been demonstrated. Typically, X-ray scattering experiments have been combined with other techniques to gain deeper insights. Schlossmann and co-workers [5] combined insights from X-ray reflectivity, GISAXS, electrocapillary curves and molecular dynamic (MD) simulations (all as a function of $\Delta_o^w \phi$) to demonstrate that hydrophobic TB^- anions in the organic phase condense onto the surface of very positively charged AuNPs coated with trimethylammonium terminated ligands at the aqueous-organic interface. Snapshots of the MD simulations at various time periods are shown in **Fig. 11**.This is strong experimental proof of the concept of TB^- acting as a “promoter”,

as described by Bell and co-workers for the case of tetrabutylammonium (TBA^+) cations condensing onto the surface of very negatively charged AuNPs [67,69]. Schlossmann and co-workers [5] show that the small 2 nm AuNPs are drawn across the interface into the low polarity organic phase by shielding their charge with hydrophobic counter-ions. Meanwhile, Vellmann *et al.* [96] utilised X-ray reflectivity, grazing incidence X-ray diffraction (GIXRD) and optical reflectance (discussed *vide infra*) as complementary techniques to independently verify the decrease in interparticle spacing and increase in AuNP surface coverage with increasing ionic strength in either the aqueous or organic phase.

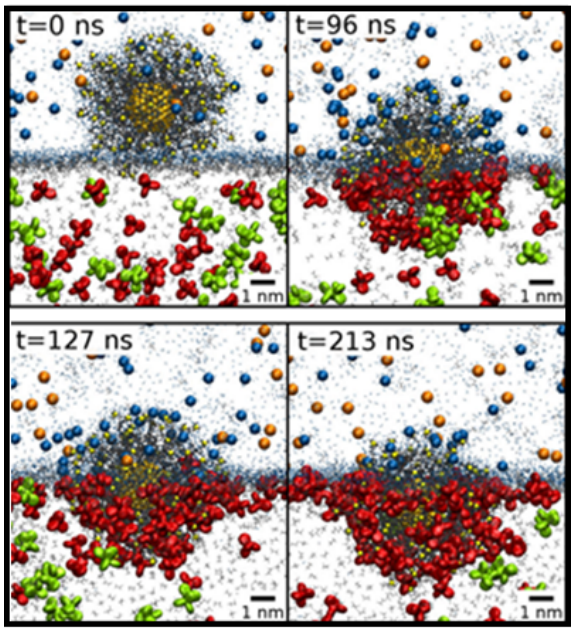

Fig. 11. Molecular dynamic (MD) simulation time sequence snapshots of the submersion of a AuNP from an aqueous (top) to an organic (bottom) electrolyte phase accompanied by the exchange of loosely bound Cl^- ions (blue) in the aqueous phase for condensed organic TB^- ions (red) in the organic phase. Adapted with permission from Ref. [5]. Copyright 2014 American Chemical Society.

6.4. Optical reflectivity and scattering

Optical reflectivity measurements have been used to investigate propagating SPR due to strong plasmon coupling in densely packed interfacial gold nanofilms [54,78,116]. Using a pseudo-

Kretschmann configuration, Cohanoschi *et al.* highlighted that a 10^3 times enhancement of the interfacial fluorescence of dyes is possible at water-xylene interfaces at the surface plasmon resonance angle (θ_{SPR}) in the presence of interfacial gold nanofilms. The enhancement was attributed to the electric field enhancement in the plasmonic "hot-spots" and the reduction of the fluorescence lifetime of dye molecules in close vicinity to the metal surface [116]. θ_{SPR} is the angle of the incident light hitting the interfacial gold nanofilm that leads to a minimum (or dip) in reflectance at a specific wavelength. Also using a pseudo-Kretschmann configuration (see **Fig. 12A(i)**), Hojeij *et al.* produced clear experimental evidence of the dip in reflectance beyond the critical angle due to SPR absorption by the interfacial gold nanofilm, closely matching theoretical calculations [78], see **Fig. 12A(ii) and (iii)**.

As noted in Section 3, SPR is also sensitive to changes in refractive index of the medium, measured as the change in reflected light passing through a prism and reflected off of the back of the interfacial gold nanofilm. The "back" of the interfacial gold nanofilm can refer to the oil-side or water-side depending on the density of the chosen oil phase. Thus, a low density oil phase such as toluene will be on top of the water phase and, when illuminated from the bottom, water is at the "back" of the interfacial gold nanofilm, and *vice versa* for a high density oil phase such as α,α,α-trifluorotoluene. Therefore, SPR-based nanoplasmonic sensors based on interfacial gold nanofilms using a pseudo-Kretschmann configuration are envisioned.

Girault and co-workers developed a setup with robotic arms to change the angle of incident light hitting the interfacial gold nanofilms, shown in **Fig. 12B**. The latter setup has been used to generate optical reflectivity data allowing the quantification of the influence of a host of variables (AuNP size, interfacial surface coverage and light wavelength, polarisation and angle of incidence, presence of surfactant, applied $\Delta_o^w\phi$) on the effectiveness of variously prepared interfacial gold nanofilms to act as nanoplasmonic mirrors [3,4,79].

Smirnov *et al.* [3] probed the optical extinction and reflectance of interfacial gold nanofilms that encapsulate the entirety of an oil droplet using an *integration sphere* (**Fig. 12C**). Additionally, they imaged gold nanofilms *in situ* with μm resolution with *optical microscopy* revealing the formation of micro-scale cracks and wrinkles. Comparison of SEM and TEM images obtained

with transfer of the nanofilm on a solid substrate show similar features, confirming that the structure of the film can stay more or less intact during the transfer [3].

Finally, Vellmann *et al.* [96] used a commercial reflectivity probe positioned at 90° to the liquid-liquid interface (see **Fig. 12D**) to monitor the red-shift in SPR reflectance maxima as a result of enhanced plasmonic coupling between AuNPs due to decreasing interparticle spacing with increasing ionic strength in either the aqueous or organic phase (allowing calibration of a so-called “plasmonic ruler”).

As detailed in Section 5, decreasing the interparticle gap in a gold nanofilm causes a near-exponential increase in the sensitivity of the responses of SPR and SERS-based nanoplasmonic sensors, as well as an exponential increase in the conductivity of the gold nanofilm. Thus, the creation of calibrated plasmonic rulers using easily accessible optical spectroscopic techniques, as described by Vellmann *et al.* [96], provides a precise guide to tune the interparticle gaps through addition of salt, applying an electric field, *etc.* in real time. The latter will be hugely beneficial to tune the strength of homogeneous plasmonic hotspots, necessary to optimise the responses of nanoplasmonic sensors using floating gold nanofilms, and also as a guide to predicting the conductivity of floating gold nanofilms.

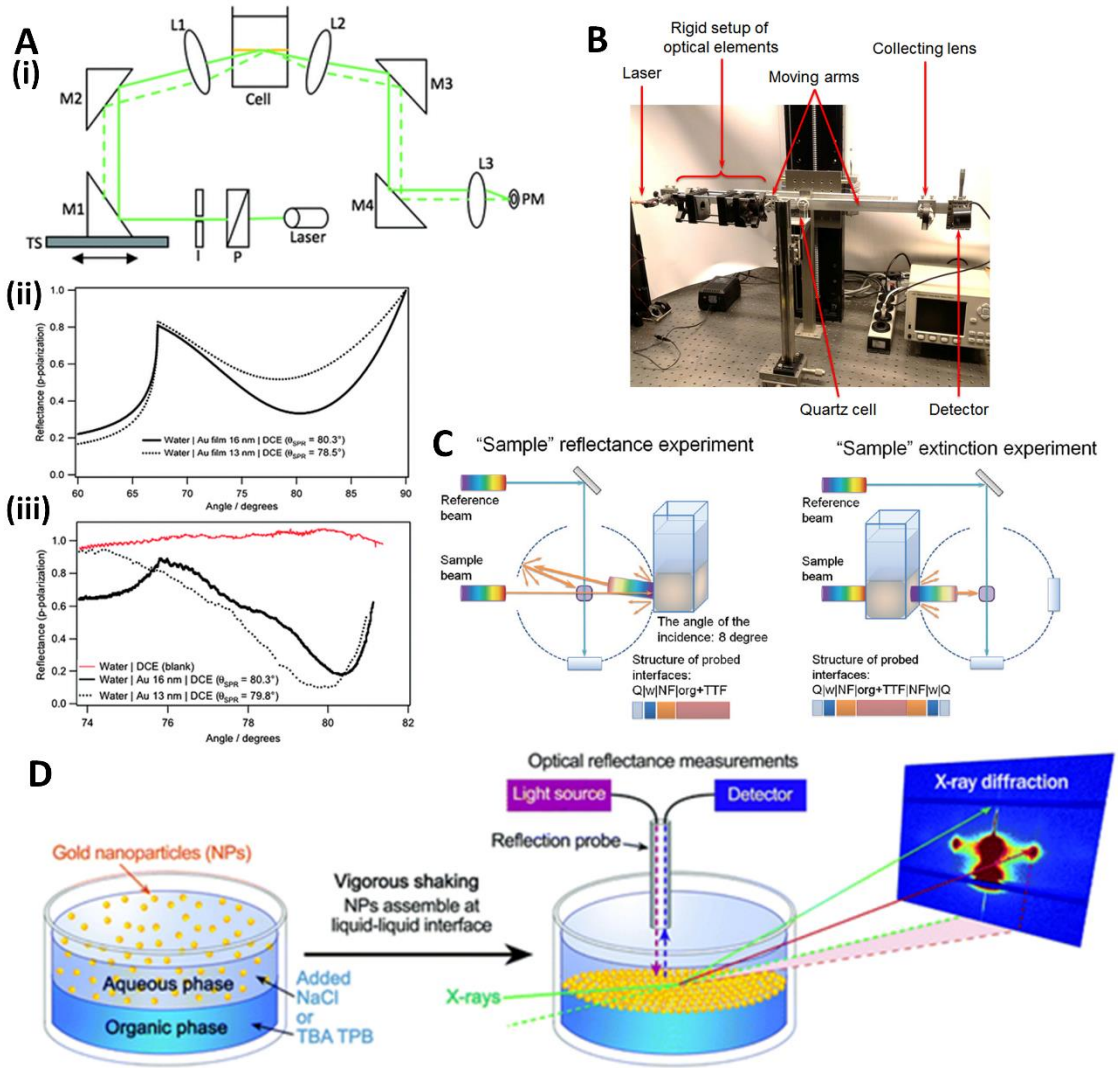

Fig. 12. (**A**)(**i**) Schematic of the experimental setup to measure surface plasmon resonance (SPR) at a gold nanofilm floating at a liquid-liquid interface using a pseudo-Kretschmann configuration. (**A**)(**ii**) Calculated and (**A**)(**iii**) experimental SPR curves for a gold nanofilm floating at a water-DCE interface for an excitation wavelength of 544 nm (full line: 16 nm Au film, dotted line: 13 nm Au film). Adapted from Ref. [78] with permission from The Royal Society of Chemistry. (**B**) Image of an experimental setup with robotic arms to investigate the angular dependence of the laser reflectance from interfacial gold nanofilms. The setup consists of robotic arms, a laser light source, various optical components and a detector, all of which move simultaneously as the angle of the laser incident to the gold nanofilms is varied. Adapted from Ref. [4] with permission from The Royal Society of Chemistry. (**C**) Reflectance and extinction spectra acquisition for interfacial gold nanofilms *in situ* by UV-Vis-NIR with a white integrating sphere. "Sample" (with the gold nanofilm coating the organic droplet) reflectance spectra were obtained at a single gold nanofilm interface on one side of the quartz cell. "Sample" extinction spectra were measured through two gold nanofilms at opposite walls of the quartz cuvette. Q, w, org, and NF, are acronyms for quartz, water, organic solvent and gold nanofilm. Adapted

from Ref. [3] with permission from The Royal Society of Chemistry. (**D**) Schematic describing the self-assembly of AuNPs at a water-DCE interface when either NaCl or tetrabutylammonium tetraphenylborate (TBATPB) was added to the aqueous or organic phase, respectively. The assembled floating gold nanofilm was analysed by X-ray reflectivity and diffraction to obtain structural information, and with optical reflectance to study the plasmon coupling between the AuNPs. Adapted from Ref. [96] with permission from The Royal Society of Chemistry.

6.5. Electrochemical techniques

Scanning electrochemical microscopy (SECM) at liquid-liquid interfaces can be used to probe the local conductivity or potentially characterise redox electrocatalysis reactions taking place at an interfacial gold nanofilm. The working principle of SECM involves the continuous recycling of a redox mediator, either in the aqueous or organic phase, between the tip of a biased micro- or nano-electrode and the surface of the interfacial gold nanofilm, see **Fig. 13A**. If a microelectrode (biased positively to oxidise the mediator) approaches an area of the interface that is non-conductive, a gradual decrease of the measured current is observed due to confinement of the semi-spherical diffusion field at the surface between the microelectrode and the liquid-liquid interface (**Fig. 13A(i)**). The latter causes a depletion of the reduced species and accumulation of oxidised species, and is called "negative feedback". A non-conductive interface can simply mean the absence of AuNPs at that local area on the interface, or the presence of AuNPs with such a large interparticle spacing that charge transport cannot propagate across the interfacial gold nanofilm. The latter was shown by Fang *et al.* where negative feedback was observed until a sufficiently large AuNP surface coverage (and therefore small interparticle distance) was reached to allow charge transport across at least μm^2-sized portions of the interfacial gold nanofilm [79], see **Fig. 13B**. For these conductive densely packed interfacial arrays of AuNPs, the measured current increases on approaching the interface as the oxidised species are re-reduced by the AuNPs (**Fig. 13(A)(ii)**). The latter is called "positive feedback" and the conductive gold nanofilm is recharged by electron injection from another redox species in the opposite phase at any point on the gold nanofilm (*i.e.,* at a considerable distance from where the microelectrode is positioned). Although as yet not demonstrated for redox electrocatalysis with gold nanofilms, in a related study, SECM has been used to monitor

photo-induced water oxidation at ITIES functionalised with nanosized bismuth vanadate ($BiVO_4$) crystals [117].

Ion transfer voltammetry can be also used to roughly estimate the surface coverage of the nanofilms. NPs adsorbed at the interface reduce the available surface area for IT, effectively blocking the surface [7]. As discussed by Amatore e*t al.* [118], a blocking layer at the electrode surface leads to an increased apparent standard rate constant for the electron transfer reaction ($k^0_{\mathrm{app}} = k^0(1-\theta)$, where θ is the surface coverage of the blocking porous layer). The same approach is true for the nanofilm covering the ITIES, see **Fig. 13C**. Hence, a simple estimation of the apparent standard ion transfer constant for the transferring ion by the method of Nicholson allows estimation of the surface coverage if the rate constant on the clean surface is known [7], see **Fig. 13D**. Other techniques successfully used to characterise the coverage of porous layers on solid electrodes, like chronoamperometry [119], could be also utilised at liquid-liquid interfaces for IT reactions.

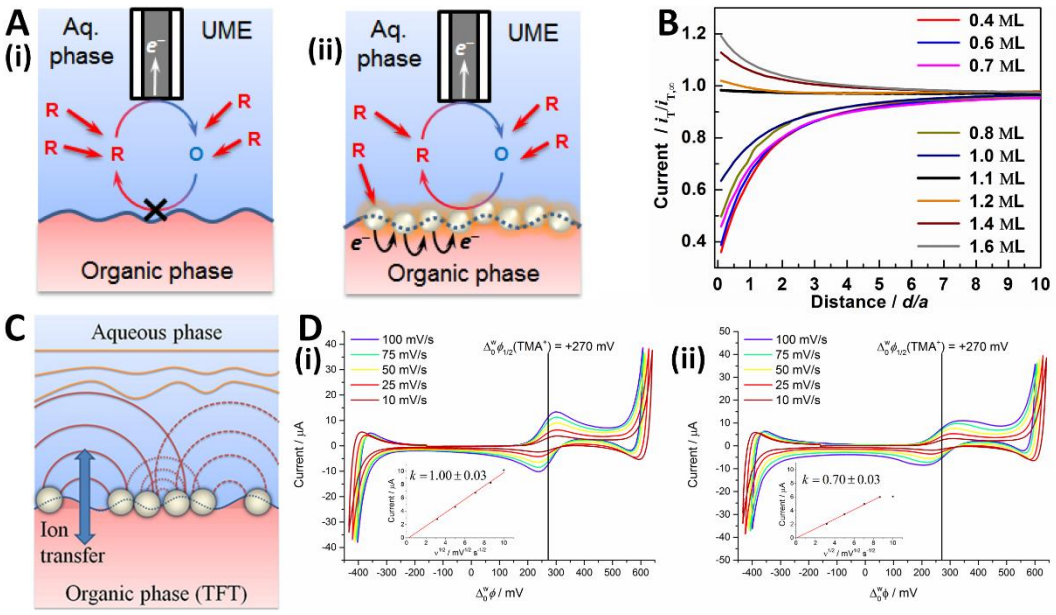

Fig. 13. Schemes of *scanning electrochemical microscopy (SECM)* experiments with (**A**) (**i**) negative feedback at a bare water-oil interface and (**ii**) positive feedback at a floating gold nanofilm at a water-oil interface. (**B**) SECM approach curves with a Pt microelectrode (radius, a,=10 μm; RG = 7) to a water-[heptane/DCE] interface in the presence of different AuNP surface

coverages. The oil phase contained 2 mM DMFc and 2 mM BATB. The translation rate was 1 μm·s^{-1}. Adapted with permission from Ref. [79]. Copyright 2013 American Chemical Society. (**C**) Schematic representation of the cross-sectional view of the ITIES partially occupied by a gold nanofilm. The lines show the diffusion profiles of ion concentration. Adapted with permission from Ref. [7]. Copyright 2015 American Chemical Society. (**D**) Ion transfer CVs (IR compensated) of 25 μM tetramethylammonium cations (TMA^+) in the aqueous phase at a water-TFT interface (**i**) without a gold nanofilm and (**ii**) with a gold nanofilm composed of 12 nm AUNPs. The apparent standard ion transfer constant (k^0_{app}) for TMA^+ was calculated by the method of Nicholson, allowing estimation of the interfacial AuNP surface coverage (θ). Adapted with permission from Ref. [7]. Copyright 2015 American Chemical Society.

6.6. Summary

Finally, a summary of the main experimental techniques used to probe AuNP adsorption at liquid-liquid interfaces, and the resulting properties of gold nanofilms formed at liquid-liquid interfaces, is provided in **Table 1**.

Table 1. Summary of experimental techniques applied to the characterization of AuNP adsorption at liquid-liquid interfaces and the properties of the resulting floating gold nanofilms.

Experimental technique	Information / Measurement Results	Ref.
Quasi-elastic light scattering (QELS)	• Monitoring the adsorption of AuNPs to the ITIES as a function of applied $\Delta^{w}_{o}\phi$ (electrocapillary curve).	[5,84]
Pendant drop tensiometry		[97–102]
Electrochemical capacitance		[77,84,103]
Surface Second Harmonic Generation (SSHG)		[85,105]
Freeze-fracture shadow casting (FreSCa) cryo-SEM	• *In situ* determination of θ_0 for AuNPs adsorbed at a liquid-liquid interface.	[108,109]
Gel-trapping techniques followed by SEM or AFM		[110]
Amplitude modulation atomic force microscopy (AFM)	• *In situ* real-space determination of interparticle separation for AuNPs adsorbed at a liquid-liquid interface.	[111]
X-ray reflectivity	• In-plane *in situ* reciprocal-space determination of interparticle separation for AuNPs adsorbed at a liquid-liquid interface. • Precise determination of AuNP out-of-plane shifts as a function of $\Delta^{w}_{o}\phi$.	[5,112]
Grazing-incidence small angle x-ray scattering (GISAXS)		[5]
Grazing incidence X-ray diffraction (GIXRD)		[96]

Molecular Dynamics (MD) simulations	• Simulation of AuNP adsorption at a liquid-liquid interface, *e.g.,* probing the influence of organic electrolyte counter-ion condensation on the surface of a AuNP during adsorption.	[5]
Reflection measurements in Pseudo-Kretschmann configuration (prism) or with robotic arms	• Angular dependence of reflectivity from floating gold nanofilms at a liquid-liquid interface at a given wavelength. • Determination of θ_{SPR}.	[4,54,78,79, 116]
UV-Vis-NIR spectroscopy with an integration sphere	• Reflectivity and extinction spectra *vs.* coverage of the interface • Monitoring red and blue-shifts of SPR and SPC extinction bands to determine *in situ* the interparticle separation for AuNPs adsorbed at a liquid-liquid interface.	[3]
Commercial reflectivity fiber probe		[96]
Scanning Electrochemical Microscopy (SECM)	• Conductivity measurements of floating gold nanofilms at the ITIES. • Probing catalytic properties of NPs adsorbed at the liquid-liquid interface.	[79,117]
Ion transfer (IT) voltammetry	• Ion permeability • Estimation of the surface coverage of AuNPs at the ITIES.	[7]

7. Perspective applications of floating gold nanofilms at the ITIES

7.1. Surface enhanced Raman spectroscopy

A series of SERS active solid electrode substrates, *e.g.,* electrically contacted lithographic nanohole and nanopore arrays [120,121], periodic particle arrays prepared by nanosphere lithography on transparent conductive oxides [122,123], or colloidal AgNP and AuNP aggregates on conductive electrodes [124,125], are suitable for electrochemical SERS (EC-SERS) applications. EC-SERS involves immersing these suitable SERS substrates in electrolyte solution and establishing an electrochemical double-layer at the substrate/electrolyte interface, the potential drop across which can be controlled externally by a potentiostat [126–128]. The ultimate goal of EC-SERS is to monitor structural changes of molecules *in situ* as they are subjected to an electric field and in some cases undergo redox processes. The insights from such experiments have tremendous potential, for example we may improve our understanding

of how a molecules redox activity is influenced by its immobilisation chemistry [129,130]. The precipitous improvement in Raman instrumentation has now reached a point that the time resolution for spectra acquisition is comparable or even shorter than the charging time of the double layer capacitance for both reversible and irreversible electrochemical processes [131]. The significance of this milestone cannot be understated as it means structural molecular information of transient intermediate species in electrochemical reactions can be directly probed *in situ*, for example during proton-coupled electron transfer reactions. The structural information gained from EC-SERS measurements can give insights that indicate potential induced (i) adsorption or desorption of molecules, (ii) molecular reorientation of molecules, (iii) rearrangement of the electrochemical double layer, or (iv) electrochemical reduction or oxidation [126].

To date, strategies to achieve EC-SERS at interfacial gold nanofilm functionalised ITIES are rare. Virtually all SERS studies involving liquid-liquid interfaces only take advantage of their inherent ability to facilitate defect-free self-assembly of floating gold nanofilms (with uniform distribution of plasmonic hot-spots), and not the ability to controllably apply a potential difference across the ITIES. For example, nanoplasmonic SERS sensors to detect epinephrine in serum, Cu^{2+}, Hg^{2+}, rhodamine 6G, malachite green, *p*-aminothiophenol and *p*-nitrothiophenol have been developed by either transferring floating gold nanofilms to silicon wafer, glass, paper or PDMS substrates (for example see **Fig. 14A**) [132–141], or by their *in situ* analysis at non-polarised water-oil interfaces (for example see **Fig. 14B**) [69,142–146]. The use of flexible PDMS substrates [132,133] is a particularly interesting strategy to vary the interparticle spacing using an external mechanical strain applied in a reversible manner (**Fig. 14C**), thereby modulating the gold nanofilms plasmonic responses (*e.g.,* towards applications in stretchable optical color filters).

The biphasic nature of SERS sensors created using floating gold nanofilms circumvents any issues regarding solubility limitations of the analyte. Both hydrophilic and hydrophobic analyte may easily come in contact with, and become pre-concentrated by attaching to, interfacial AuNPs during emulsification by sonication. Thus, simultaneous multiphase analyte detection is possible [143]. Additionally, tailored detection strategies can be developed to facilitate large

SERS enhancements involving oil-based hydrophobic ligands binding hydrophilic target aqueous analytes (such as heavy metal ions) at the liquid-liquid interface during emulsification [145]. Ideally, as shown in **Fig. 14D**, interfacial metal-ligand binding and attachment of the metal-ligand complexes to the interfacial AuNPs occurs simultaneously.

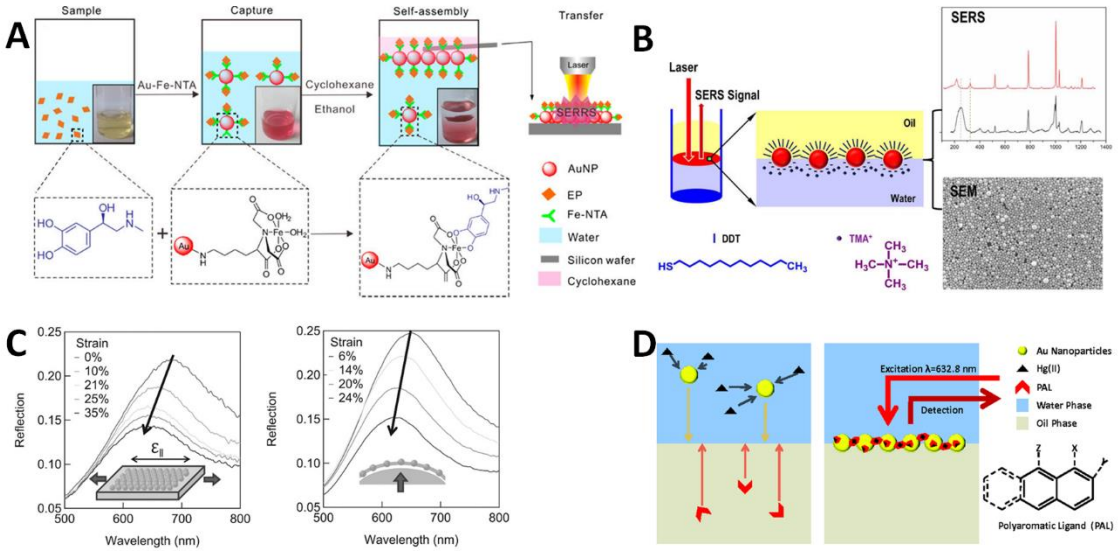

Fig. 14. Current state-of-the-art surface enhanced Raman spectroscopy (SERS) studies utilising liquid-liquid interfaces. (**A**) Schematic representation of the detection process for epinephrine (EP) by a 2D surface enhanced resonance Raman spectroscopy (SERRS) platform. The *sample* contains EP in serum (so an aqueous solution), to which AuNPs modified with α,β- nitriloacetic acid and $Fe(NO_3)_3$ are added. The modified AuNPs *capture* the EP and *self-assembly* (due to addition of ethanol) at the water-cyclohexane interface. The self-assembled gold nanofilms, enriched with the target EP analyte, are *transferred* to a silicon substrate for *ex situ* SERRS analysis. Adapted with permission from Ref. [135]. Copyright 2017 American Chemical Society. (**B**) A gold nanofilm was formed at the water-toluene interface by addition of 1- dodecanethiol (DDT) and TMA^+ ions to the biphasic cell. *In situ* SERS analysis at the liquid-liquid interface demonstrated that the interfacial morphology of the gold nanofilm was closely linked to its chemical environmental (*e.g.,* in the presence of TMA^+ alone, with varying amounts of DDT present, *etc.*). Adapted with permission from Ref. [146]. Copyright 2015 American Chemical Society. (**C**) Reflection spectra of AuNP mats under increasing strain. The AuNP mats were prepared by transferring a floating gold nanofilm formed at a water-hexane interface to a flexible PDMS substrate. (Left panel) Uniaxial stretch parallel to optical polarisation and (right panel) biaxial uniform stretch with unpolarised light. The discrepancy in intensity if due to the curved film on the lens surface. Adapted from Ref. [132], with the permission of AIP Publishing. (**D**) An aqueous phase containing AuNPs and a heavy metal ion target analyte (*e.g.,* Hg^{2+}) are placed in contact with an oil phase containing a dissolved polyaromatic ligand (PAL). Shaking

creates a biphasic emulsion, causing all aqueous and organic species present to self-assembly at the common liquid-liquid interface. After assembly, Hg^{2+} can be detected sensitively by SERS through its effects on the *in situ* SERS signals from the PAL molecules attached to the AuNPs surface adsorbed at the interface. Adapted with permission from Ref. [145]. Copyright 2014 Wiley-VCH.

In this perspective section, we denote experiments that combine an external manipulation of $\Delta_o^w\phi$ with a potentiostat and simultaneous SERS measurements *in situ* at the ITIES as EC-SERS@ITIES. The only report to date of EC-SERS@ITIES is that by Booth *et al.* [147]. In that study, citrate stabilised AgNPs were reversibly adsorbed and desorbed from the ITIES for a finite number of cycles by varying $\Delta_o^w\phi$ negatively and positively, respectively. Upon AgNP adsorption at negative potentials a sharp increase in the SERS intensity of the lipophilic organic cation BA^+ was detected. This observation corresponds very well with that by Schlossmann and co-workers [5] (described *vide supra*) of organic counter-ion condensation onto highly charged AuNPs overcoming the electrostatic barrier presented by the low permittivity organic material at the ITIES during potential-induced adsorption events. Thus, EC-SERS@ITIES can be used to sensitively detect organic ions of opposite charge to the stabilising ligand on interfacially adsorbed plasmonic NPs.

Many other possibilities of EC-SERS@ITIES have yet to be explored. For example, certain charged species (*i.e.,* ions) in either the aqueous or organic phase can be transferred reversibly over and back across the ITIES by varying $\Delta_o^w\phi$. Each ion will undergo IT at a signature formal ion transfer potential ($\Delta_o^w\phi^{0'}$) that is a measure of the Gibbs energy of transfer for that ion expressed on the voltage scale and depends heavily on the charge and chemical structure of the ion [9]. Thus, certain ions in a mixture can be selectively transferred over and back across the ITIES by matching the applied $\Delta_o^w\phi$ with the $\Delta_o^w\phi^{0'}$ for that ion. Therefore, in theory, the SERS signal for the selected ion undergoing IT will be transiently enhanced as it traverses the ITIES through the hot-spots between interfacial AuNPs in the floating gold nanofilms. Indeed, Smirnov *et al.* have demonstrated that the presence of an interfacial gold nanofilm does not impede IT for model ions such as tetramethylammonium cations (TMA^+) [7]. Further strategies may be explored that combine the demonstrated ability to achieve electrocatalysis at gold

nanofilms with the plasmonic enhancement at the hot-spots between the AuNPs. For example, the redox active dye Nile Blue is a very popular probe in EC-SERS studies as its oxidised form undergoes resonant excitation at 633 nm, giving a strong SERS signal, but its reduced form is non-resonant leading to a weak SERS signal [126]. Thus, the oxidised and reduced forms of this species are readily distinguishable by SERS. As a proof-of-concept, the analogous EC-SERS@ITIES experiment may involve the reduction of the oxidised form of Nile Blue in the aqueous phase *via* AuNP mediated IET from an electron donor species in the oil phase (such as decamethylferrocene). The thermodynamics of IET would be controlled by external application of $\Delta_o^w\phi$ by the potentiostat and the disappearance of the oxidised dye signal monitored *in situ* by SERS.

7.2. Electrovariable nanofilms

As noted in section 4, to date, the precise experimental conditions to reversibly adsorb/desorb gold nanofilms composed of relatively large AuNPs (*e.g.,* in the size range of 10 to 60 nm) by tuning $\Delta_o^w\phi$ have not been identified. Indeed, reversible stimulus-induced self-assembly of NPs on 2-D interfaces is difficult to achieve and examples in the literature are few. Sashuk *et al.* reported the dynamic self-assembly of amphiphilic and uncharged NPs dispersed at an air-water interface in response to changes in the gradient of $\gamma_{w/o}$ [148]. The gradient was changed by either adding or removing organic solvent on the fluid interface, causing the NPs to compress into local dense spots. Once the gradient of $\gamma_{w/o}$ dissipated, the compressed AuNPs disassembled [148]. Ding *et al.* dynamically tuned the distance between the AuNPs in a floating gold nanofilm (and hence the nanofilm's optical properties) by rapid, repeatable expansion and contraction of poly-N-isopropylacrylamide (PNIPAM) nanocoatings on the AuNPs at different temperatures [75]. Meanwhile, as discussed, Bera *et al.* have definitively shown that the dynamic lateral movement of AuNPs at the interface is possible by tuning $\Delta_o^w\phi$ [5], a much more convenient external stimulus to employ in possible electrovariable optical devices than the introduction/removal of solvent or varying temperature.

Recently, Gschwend *et al.* have created so called "electrovariable Marangoni shutters" [4]. The concept harnesses known changes in $\gamma_{w/o}$ that can be reversibly induced at the liquid-liquid

interface as a function of $\Delta_o^w\phi$ in the presence of an anionic surfactant (sodium dodecyl sulfate (SDS)) that undergoes IT. The interplay of adsorption-desorption and IT as a function of $\Delta_o^w\phi$ causes instabilities or Marangoni-type movements (*i.e.,* mass transfer along an interface between two fluids due to a surface tension gradient) [149–151]. The AuNPs in the gold nanofilm are swept up in these Marangoni-type movements, always moving to regions of higher $\gamma_{w/o}$. Indeed, the AuNPs may be induced to either reversibly crowd around the periphery of the interface (leading to the shutter being "off" with the majority of the interface non-reflective) or spread uniformly across the interface (leading to the shutter being "on" and the interface highly reflective) as a function of $\Delta_o^w\phi$ [4], see **Fig. 15**. The distribution of the electric field at the ITIES is critically dependent on the shape and position of the platinum counter electrodes on either side of the liquid-liquid interface. As a result, by manipulating the latter, further enhanced control over the spatial regions on the interface where the Marangoni-effects are felt strongest, and thus where the AuNPs can be induced to assembly more densely, will be possible.

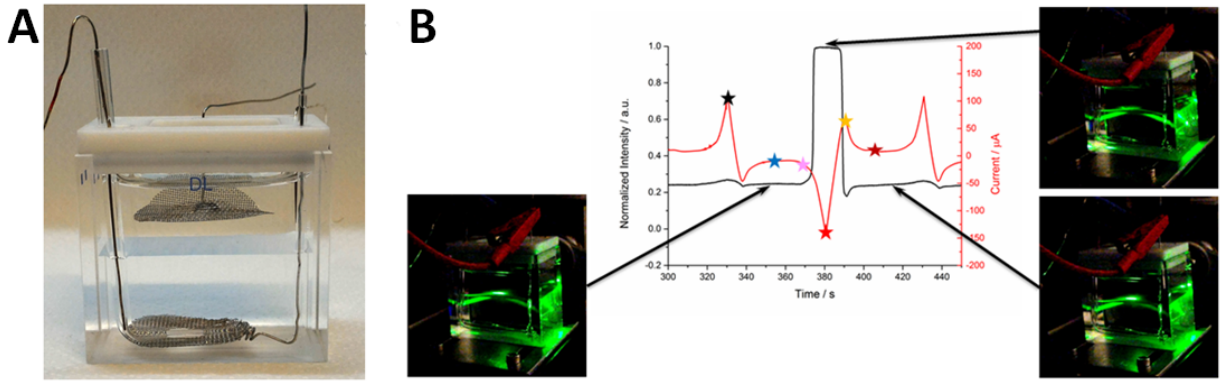

Fig. 15. Electrovariable Marangoni shutters with floating gold nanofilms at the ITIES. (**A**) Silanised four-electrode electrochemical cell in a quartz rectangular cuvette with large Pt-mesh aqueous and organic counter electrodes, and an extremely flat and smooth water-TFT interface (critical for reflectance measurements). (**B**) Monitoring the intensity of light reflected from the centre of a water-TFT interface (black line) as a function of $\Delta_o^w\phi$, varied by cyclic voltammetry (CV; red line). The light was incident on the water-TFT interface at 66°, *i.e.,* below the critical angle for total internal reflection (TIR). The black star on the CV represents a positive $\Delta_o^w\phi$, with the current increasing at this point positively due to the transfer of residual metal cations to the oil phase. After this point $\Delta_o^w\phi$ was scanned to more negative values, immediately causing a dip

in the current negatively as metal cations transferred back from the oil into the water phase. The blue and pink stars represent two progressively more negative potentials in the middle of the PPW as $\Delta_o^w\phi$ was scanned negatively. At very positive $\Delta_o^w\phi$ and at $\Delta_o^w\phi$ values spanning the centre of the PPW (*i.e.,* the region between the black and pink stars), the AuNPs were seen to be distributed around the perimeter of the quartz cuvette. Thus, a low reflectance was measured in this potential range (also seen by eye in a video snapshot, bottom-left image). Once $\Delta_o^w\phi$ was scanned to a very negative value (red star), the anionic surfactant SDS transferred from the water to oil phase leading to a large negative increase in current. Immediately, AuNPs were seen to migrate to the centre of the water-oil interface, rapidly accumulating and causing a huge increase in reflectance (seen by eye in top-right image). Once more, after this point $\Delta_o^w\phi$ was switched in the positive direction causing the SDS to move from back from the oil to water phase, producing a positive current. The increased reflectance was maintained until all SDS ions were transferred back into the water phase (yellow star). Finally, as $\Delta_o^w\phi$ was scanned positively to $\Delta_o^w\phi$ values once more in the centre of the PPW (dark red star), the system returned to its initial state with the AuNPs again crowded around the periphery of the quartz cuvette and the reflectance greatly diminished (seen by eye in bottom-right image). Adapted from Ref. [4] with permission from The Royal Society of Chemistry.

A major factor when designing electrovariable optics based on dynamic self-assembly of NPs will be response time to the external stimulus (*i.e.,* the applied electric field especially, but also perhaps temperature or light) [53]. With regard to the reversible adsorption and desorption of gold nanofilms from the ITIES, the response time will be limited by the rate of diffusion of AuNPs in the bulk liquid towards the interface and back-off again. Thus, the time-constant for observable "on/off" behaviour could be tens of minutes depending on the concentration and diffusion coefficient of the AuNPs in the bulk phase, and their size [53]. Such response times may be suitable for niche applications, *e.g.,* windows in large buildings that gradually become more or less reflective to help equalise the temperature at a desired level as the intensity of sunlight rises and drops during the day. Realistically, however, for more general applications the time-constant for observable "on/off" behaviour needs to be reduced to second or ideally millisecond regimes. In this regard, the near instantaneous "on/off" behaviour observed by Gschwend *et al.* [4] for lateral movement of the AuNPs across the fluidic interface is hugely encouraging. Thus, building on this initial premise of combining interfacial gold nanofilms and charged surfactant at an ITIES, rapid response electrovariable optics for mirror and filters applications will be within reach in the short-term.

8. Conclusions

To conclude, the practical utility of floating gold nanofilms is already being realised in the analytical chemistry community for SERS sensor applications. However, approaches to date have broadly been limited in scope to using liquid-liquid interfaces for bottom-up self-assembly purposes only. Major advances in SERS and SPR sensors can be made by simultaneously harnessing the aspects of AuNP self-assembly and controllably applying electric fields at the gold nanofilm functionalised ITIES. In this way, for example, the electrocatalytic properties of AuNPs can be utilised in conjunction with their nanoplasmonic properties to create truly unique sensors in a new branch of SERS we call EC-SERS@ITIES. Immediate applications of floating gold nanofilms in rapid response electrovariable optic devices are now within reach thanks to pioneering simulation studies and recent experimental breakthroughs. Finally, while this review is limited to discussing simple AuNPs, the potential utility and impact of ITIES functionalised with gold (or any other metal) nanorods, nano-triangles, nanocubes, core-shell NPs, Janus NPs, carbon supported NPs, semiconductors *etc.*, for electrocatalytic, nanoplasmonic and electrovariable optic applications has barely been scratched and represents an exciting research avenue for the future.

Acknowledgements

This publication has emanated from research by M.D.S. supported in part by a research grant from Science Foundation Ireland (SFI) under Grant Number 13/SIRG/2137. T.J.S is grateful to the European Commission for a H2020-MSCA-IF grant, project number nanoOIPC-DLV-708814. P.P. acknowledges the financial support from the Swiss National Science Foundation under Grant Ambizione Energy 160553.

References

[1] L. Hu, M. Chen, X. Fang, L. Wu, Oil–water interfacial self-assembly: a novel strategy for nanofilm and nanodevice fabrication, Chem. Soc. Rev. 41 (2012) 1350–1362. doi:10.1039/c1cs15189d.

[2] J.B. Edel, A.A. Kornyshev, A.R. Kucernak, M. Urbakh, Fundamentals and applications of self-assembled plasmonic nanoparticles at interfaces, Chem. Soc. Rev. 45 (2016) 1581–1596. doi:10.1039/C5CS00576K.
[3] E. Smirnov, P. Peljo, M.D. Scanlon, F. Gumy, H.H. Girault, Self-healing gold mirrors and filters at liquid–liquid interfaces, Nanoscale. 8 (2016) 7723–7737. doi:10.1039/C6NR00371K.
[4] G.C. Gschwend, E. Smirnov, P. Peljo, H.H. Girault, Electrovariable Gold Nanoparticle Films at Liquid-Liquid Interfaces: from redox electrocatalysis to Marangoni-shutters, Faraday Discuss. (2017). doi:10.1039/C6FD00238B.
[5] M.K. Bera, H. Chan, D.F. Moyano, H. Yu, S. Tatur, D. Amoanu, W. Bu, V.M. Rotello, M. Meron, P. Král, B. Lin, M.L. Schlossman, Interfacial Localization and Voltage-Tunable Arrays of Charged Nanoparticles, Nano Lett. 14 (2014) 6816–6822. doi:10.1021/nl502450j.
[6] E. Smirnov, P. Peljo, M.D. Scanlon, H.H.H. Girault, Gold Nanofilm Redox Catalysis for Oxygen Reduction at Soft Interfaces, Electrochim. Acta. 197 (2016) 362–373. doi:10.1016/j.electacta.2015.10.104.
[7] E. Smirnov, P. Peljo, M.D. Scanlon, H.H. Girault, Interfacial Redox Catalysis on Gold Nanofilms at Soft Interfaces, ACS Nano. 9 (2015) 6565–6575. doi:10.1021/acsnano.5b02547.
[8] Y. Gründer, M.D. Fabian, S.G. Booth, D. Plana, D.J. Fermín, P.I. Hill, R.A.W. Dryfe, Solids at the liquid-liquid interface: Electrocatalysis with pre-formed nanoparticles, Electrochim. Acta. 110 (2013) 809–815. doi:10.1016/j.electacta.2013.03.185.
[9] P. Peljo, H.H. Girault, Liquid/Liquid Interfaces, Electrochemistry at, in: Encyclopedia of Analytical Chemistry, John Wiley & Sons, Ltd, Chichester, UK, 2012. doi:10.1002/9780470027318.a5306.pub2.
[10] Z. Samec, Electrochemistry at the interface between two immiscible electrolyte solutions (IUPAC Technical Report), Pure Appl. Chem. 76 (2004) 2147–2180. doi:10.1351/pac200476122147.
[11] Z. Samec, J. Langmaier, T. Kakiuchi, Charge-transfer processes at the interface between hydrophobic ionic liquid and water, Pure Appl. Chem. 81 (2009) 1473–1488. doi:10.1351/PAC-CON-08-08-36.
[12] N.E.A. Cousens, A.R. Kucernak, Electrochemistry of the ionic liquid|oil interface: A new water-free interface between two immiscible electrolyte solutions, Electrochem. Commun. 31 (2013) 63–66. doi:10.1016/j.elecom.2013.03.002.
[13] D. Michael, I. Benjamin, Molecular dynamics simulation of the water|nitrobenzene interface, J. Electroanal. Chem. 450 (1998) 335–345. doi:10.1016/S0022-0728(97)00653-0.
[14] T.J. Stockmann, R. Guterman, P.J. Ragogna, Z. Ding, Trends in Hydrophilicity/Lipophilicity of Phosphonium Ionic Liquids As Determined by Ion-Transfer Electrochemistry, Langmuir. 32 (2016) 12966–12974. doi:10.1021/acs.langmuir.6b03031.
[15] T.J. Stockmann, A.M. Montgomery, Z. Ding, Determination of alkali metal ion transfers at liquid|liquid interfaces stabilized by a micropipette, J. Electroanal. Chem. 684 (2012) 6–12. doi:10.1016/j.jelechem.2012.08.013.
[16] A.J. Olaya, M.A. Méndez, F. Cortes-Salazar, H.H. Girault, Voltammetric determination of extreme standard Gibbs ion transfer energy, J. Electroanal. Chem. 644 (2010) 60–66. doi:10.1016/j.jelechem.2010.03.030.
[17] B. Hundhammer, C. Müller, T. Solomon, H. Alemu, H. Hassen, Ion transfer across the water-o-dichlorobenzene interface, J. Electroanal. Chem. 319 (1991) 125–135. doi:10.1016/0022-0728(91)87072-C.
[18] P. Peljo, L. Qiao, L. Murtomäki, C. Johans, H.H. Girault, K. Kontturi, Electrochemically controlled proton-transfer-catalyzed reactions at liquid-liquid interfaces: Nucleophilic substitution on ferrocene methanol, ChemPhysChem. 14 (2013) 311–314. doi:10.1002/cphc.201200953.
[19] A.J. Olaya, P. Ge, H.H. Girault, Ion transfer across the water|trifluorotoluene interface,

Electrochem. Commun. 19 (2012) 101–104. doi:10.1016/j.elecom.2012.03.010.
[20] T.J. Stockmann, J.M. Noël, A. Abou-Hassan, C. Combellas, F. Kanoufi, Facilitated Lewis Acid Transfer by Phospholipids at a (Water|CHCl3) Liquid|Liquid Interface toward Biomimetic and Energy Applications, J. Phys. Chem. C. 120 (2016) 11977–11983. doi:10.1021/acs.jpcc.6b02354.
[21] H. Ohde, A. Uehara, Y. Yoshida, K. Maeda, S. Kihara, Some factors in the voltammetric measurement of ion transfer at the micro aqueous|organic solution interface, J. Electroanal. Chem. 496 (2001) 110–117. doi:10.1016/S0022-0728(00)00367-3.
[22] M. Kasuno, Y. Matsuyama, M. Iijima, Voltammetry of Ion Transfer at a Water-Toluene Micro-Interface, ChemElectroChem. 3 (2016) 694–697. doi:10.1002/celc.201500568.
[23] Z. Samec, V. Mareček, J. Weber, Charge transfer between two immiscible electrolyte solutions: Part IV. Electron transfer between hexacyanoferrate(III) in water and ferrocene in nitrobenzene investigated by cyclic voltammetry with four-electrode system, J. Electroanal. Chem. 103 (1979) 11–18. doi:10.1016/S0022-0728(79)80475-1.
[24] J.D. Watkins, F. Amemiya, M. Atobe, P.C. Bulman-Page, F. Marken, Liquid | liquid biphasic electrochemistry in ultra-turrax dispersed acetonitrile | aqueous electrolyte systems, Electrochim. Acta. 55 (2010) 8808–8814. doi:10.1016/j.electacta.2010.07.104.
[25] J.C. Hidalgo-Acosta, M. a. Méndez, M.D. Scanlon, H. Vrubel, V. Amstutz, W. Adamiak, M. Opallo, H.H. Girault, Catalysis of water oxidation in acetonitrile by iridium oxide nanoparticles, Chem. Sci. 6 (2015) 1761–1769. doi:10.1039/C4SC02196G.
[26] E. Smirnov, P. Peljo, H.H. Girault, Self-assembly and redox induced phase transfer of gold nanoparticles at a water–propylene carbonate interface, Chem. Commun. 53 (2017) 4108–4111. doi:10.1039/C6CC09638G.
[27] Z. Samec, Dynamic electrochemistry at the interface between two immiscible electrolytes, Electrochim. Acta. 84 (2012) 21–28. doi:10.1016/j.electacta.2012.03.118.
[28] D.W.M. Arrigan, G. Herzog, Theory of electrochemistry at miniaturised interfaces between two immiscible electrolyte solutions, Curr. Opin. Electrochem. 1 (2017) 66–72. doi:10.1016/j.coelec.2017.01.003.
[29] D.W.M. Arrigan, Y. Liu, Electroanalytical Ventures at Nanoscale Interfaces Between Immiscible Liquids, Annu. Rev. Anal. Chem. 9 (2016) 145–161. doi:10.1146/annurev-anchem-071015-041415.
[30] V. Mareček, Z. Samec, Ion transfer kinetics at the interface between two immiscible electrolyte solutions supported on a thick-wall micro-capillary. A mini review, Curr. Opin. Electrochem. (2017). doi:10.1016/j.coelec.2016.11.004.
[31] D.W.M. Arrigan, E. Alvarez de Eulate, Y. Liu, Electroanalytical Opportunities Derived from Ion Transfer at Interfaces between Immiscible Electrolyte Solutions, Aust. J. Chem. 69 (2016) 1016–1032. doi:10.1071/CH15796.
[32] P. Peljo, M.D. Scanlon, A.J. Olaya, L. Rivier, E. Smirnov, H.H. Girault, Redox electrocatalysis of floating nanoparticles: determining electrocatalytic properties without the influence of solid supports, J. Phys. Chem. Lett. (2017) Submitted.
[33] V.R. Stamenkovic, D. Strmcnik, P.P. Lopes, N.M. Markovic, Energy and fuels from electrochemical interfaces, Nat. Mater. 16 (2017) 57–69. doi:10.1038/nmat4738.
[34] N. Ostojic, R.M. Crooks, Electrocatalytic Reduction of Oxygen on Platinum Nanoparticles in the Presence and Absence of Interactions with the Electrode Surface, Langmuir. 32 (2016) 9727–9735. doi:10.1021/acs.langmuir.6b02578.
[35] J. Herranz, J. Durst, E. Fabbri, A. Patru, X. Cheng, A.A. Permyakova, T.J. Schmidt, Interfacial effects on the catalysis of the hydrogen evolution, oxygen evolution and CO2-reduction reactions for (co-)electrolyzer development, Nano Energy. 29 (2016) 4–28. doi:10.1016/j.nanoen.2016.01.027.
[36] B.E. Hayden, Particle Size and Support Effects in Electrocatalysis, Acc. Chem. Res. 46 (2013) 1858–

1866. doi:10.1021/ar400001n.
[37] M.D. Scanlon, P. Peljo, M.A. Méndez, E. Smirnov, H.H. Girault, Charging and discharging at the nanoscale: Fermi level equilibration of metallic nanoparticles, Chem. Sci. 6 (2015) 2705–2720. doi:10.1039/C5SC00461F.
[38] S.K. Ghosh, T. Pal, Interparticle Coupling Effect on the Surface Plasmon Resonance of Gold Nanoparticles: From Theory to Applications, Chem. Rev. 107 (2007) 4797–4862. doi:10.1021/cr0680282.
[39] Z. Yang, S. Chen, P. Fang, B. Ren, H.H. Girault, Z. Tian, LSPR properties of metal nanoparticles adsorbed at a liquid–liquid interface, Phys. Chem. Chem. Phys. 15 (2013) 5374–5378. doi:10.1039/c3cp44101f.
[40] S. Kadkhodazadeh, T. Christensen, M. Beleggia, N.A. Mortensen, J.B. Wagner, The Substrate Effect in Electron Energy-Loss Spectroscopy of Localized Surface Plasmons in Gold and Silver Nanoparticles, ACS Photonics. 4 (2017) 251–261. doi:10.1021/acsphotonics.6b00489.
[41] M.A. Mahmoud, M.A. El-Sayed, Substrate Effect on the Plasmonic Sensing Ability of Hollow Nanoparticles of Different Shapes, J. Phys. Chem. B. 117 (2013) 4468–4477. doi:10.1021/jp3085793.
[42] M.A. Mahmoud, M. Chamanzar, A. Adibi, M.A. El-Sayed, Effect of the Dielectric Constant of the Surrounding Medium and the Substrate on the Surface Plasmon Resonance Spectrum and Sensitivity Factors of Highly Symmetric Systems: Silver Nanocubes, J. Am. Chem. Soc. 134 (2012) 6434–6442. doi:10.1021/ja300901e.
[43] M.W. Knight, Y. Wu, J.B. Lassiter, P. Nordlander, N.J. Halas, Substrates matter: influence of an adjacent dielectric on an individual plasmonic nanoparticle, Nano Lett. 9 (2009) 2188–2192. doi:10.1021/nl900945q.
[44] E. Ringe, J.M. McMahon, K. Sohn, C. Cobley, Y. Xia, J. Huang, G.C. Schatz, L.D. Marks, R.P. Van Duyne, Unraveling the Effects of Size, Composition, and Substrate on the Localized Surface Plasmon Resonance Frequencies of Gold and Silver Nanocubes: A Systematic Single-Particle Approach, J. Phys. Chem. C. 114 (2010) 12511–12516. doi:10.1021/jp104366r.
[45] P.L. Stiles, J.A. Dieringer, N.C. Shah, R.P. Van Duyne, Surface-Enhanced Raman Spectroscopy, Annu. Rev. Anal. Chem. 1 (2008) 601–626. doi:10.1146/annurev.anchem.1.031207.112814.
[46] K. Mayer, J. Hafner, Localized surface plasmon resonance sensors, Chem. Rev. 111 (2011) 3828–3857. doi:10.1021/cr100313v.
[47] O. Kedem, A. Vaskevich, I. Rubinstein, Improved Sensitivity of Localized Surface Plasmon Resonance Transducers Using Reflection Measurements, J. Phys. Chem. Lett. 2 (2011) 1223–1226. doi:10.1021/jz200482f.
[48] M.E. Flatté, A.A. Kornyshev, M. Urbakh, Nanoparticles at electrified liquid–liquid interfaces: new options for electro-optics, Faraday Discuss. 143 (2009) 109–115. doi:10.1039/b901253m.
[49] M.E. Flatté, A.A. Kornyshev, M. Urbakh, Electrovariable nanoplasmonics and self-assembling smart mirrors, J. Phys. Chem. C. 114 (2010) 1735–1747. doi:10.1021/jp9083234.
[50] A.A. Kornyshev, M. Marinescu, J. Paget, M. Urbakh, Reflection of light by metal nanoparticles at electrodes, Phys. Chem. Chem. Phys. 14 (2012) 1850–1859. doi:10.1039/c1cp22680k.
[51] J. Paget, V. Walpole, M. Blancafort Jorquera, J.B. Edel, M. Urbakh, A.A. Kornyshev, A. Demetriadou, Optical properties of ordered self-assembled nanoparticle arrays at interfaces, J. Phys. Chem. C. 118 (2014) 23264–23273. doi:10.1021/jp5071192.
[52] D. Sikdar, A.A. Kornyshev, Theory of tailorable optical response of two-dimensional arrays of plasmonic nanoparticles at dielectric interfaces, Sci. Rep. 6 (2016) 33712. doi:10.1038/srep33712.
[53] D. Sikdar, A.O. Bucher, C. Zagar, A.A. Kornyshev, Electrochemical plasmonic metamaterials: Towards fast electro-tuneable reflecting nanoshutters, Faraday Discuss. (2017). doi:10.1039/C6FD00249H.

[54] D. Schaming, M. Hojeij, N. Younan, H. Nagatani, H.J. Lee, H.H. Girault, Photocurrents at polarized liquid|liquid interfaces enhanced by a gold nanoparticle film, Phys. Chem. Chem. Phys. 13 (2011) 17704–17711. doi:10.1039/c1cp22072a.
[55] H. Nagatani, S. Tonari, T. Shibata, T. Sagara, Gold nanoparticles-enhanced photocurrent at a dye-sensitized liquid|liquid interface, Electrochem. Commun. 13 (2011) 985–988. doi:10.1016/j.elecom.2011.06.018.
[56] D. Schaming, I. Hatay, F. Cortez, A. Olaya, M. a Méndez, P.Y. Ge, H. Deng, P. Voyame, Z. Nazemi, H. Girault, Artificial photosynthesis at soft interfaces., Chimia 65 (2011) 356–359. doi:10.2533/chimia.2011.356.
[57] R. Lahtinen, D.J. Fermín, K. Kontturi, H.H. Girault, Artificial photosynthesis at liquid|liquid interfaces: Photoreduction of benzoquinone by water soluble porphyrin species, J. Electroanal. Chem. 483 (2000) 81–87. doi:10.1016/S0022-0728(99)00505-7.
[58] S.G. Booth, R.A.W. Dryfe, Assembly of Nanoscale Objects at the Liquid/Liquid Interface, J. Phys. Chem. C. 119 (2015) 23295–23309. doi:10.1021/acs.jpcc.5b07733.
[59] R.A.W. Dryfe, A. Uehara, S.G. Booth, Metal Deposition at the Liquid-Liquid Interface, Chem. Rec. 14 (2014) 1013–1023. doi:10.1002/tcr.201402027.
[60] F. Reincke, S.G. Hickey, W.K. Kegel, D. Vanmaekelbergh, Spontaneous Assembly of a Monolayer of Charged Gold Nanocrystals at the Water/Oil Interface, Angew. Chemie - Int. Ed. 43 (2004) 458–462. doi:10.1002/anie.200352339.
[61] H. Duan, D. Wang, D.G. Kurth, H. Möhwald, Directing self-assembly of nanoparticles at water/oil interfaces, Angew. Chemie - Int. Ed. 43 (2004) 5639–5642. doi:10.1002/anie.200460920.
[62] W.H. Binder, Supramolecular assembly of nanoparticles at liquid-liquid interfaces, Angew. Chemie - Int. Ed. 44 (2005) 5172–5175. doi:10.1002/anie.200501220.
[63] F. Reincke, W.K. Kegel, H. Zhang, M. Nolte, D. Wang, D. Vanmaekelbergh, H. Möhwald, Understanding the Self-Assembly of Charged Nanoparticles at the Water/Oil Interface, Phys. Chem. Chem. Phys. 8 (2006) 3828–3835. doi:10.1039/b604535a.
[64] D. Wang, H. Duan, H. Möhwald, The water/oil interface: the emerging horizon for self-assembly of nanoparticles, Soft Matter. 1 (2005) 412–416. doi:10.1039/b511911a.
[65] M.E. Flatté, A.A. Kornyshev, M. Urbakh, Understanding voltage-induced localization of nanoparticles at a liquid–liquid interface, J. Phys. Condens. Matter. 20 (2008) 73102. doi:10.1088/0953-8984/20/7/073102.
[66] E. Smirnov, M.D. Scanlon, D. Momotenko, H. Vrubel, M.A. Méndez, P.-F. Brevet, H.H. Girault, D. Scanlon, D. Momotenko, H. Vrubel, M.A. Me, Gold Metal Liquid-Like Droplets, ACS Nano. 8 (2014) 9471–9481. doi:10.1021/nn503644v.
[67] Y. Xu, M.P. Konrad, W.W.Y. Lee, Z. Ye, S.E.J. Bell, A Method for Promoting Assembly of Metallic and Nonmetallic Nanoparticles into Interfacial Monolayer Films, Nano Lett. 16 (2016) 5255–5260. doi:10.1021/acs.nanolett.6b02418.
[68] Y. Xu, M.P. Konrad, J.L. Trotter, C.P. McCoy, S.E.J. Bell, Rapid One-Pot Preparation of Large Freestanding Nanoparticle-Polymer Films, Small. 13 (2017) 1602163. doi:10.1002/smll.201602163.
[69] M.P. Konrad, A.P. Doherty, S.E.J. Bell, Stable and uniform SERS signals from self-assembled two-dimensional interfacial arrays of optically coupled Ag nanoparticles, Anal. Chem. 85 (2013) 6783–6789. doi:10.1021/ac4008607.
[70] V.A. Turek, M.P. Cecchini, J. Paget, A.R. Kucernak, A.A. Kornyshev, J.B. Edel, Plasmonic Ruler at the Liquid–Liquid Interface, ACS Nano. 6 (2012) 7789–7799. doi:10.1021/nn302941k.
[71] M. Luo, G.K. Olivier, J. Frechette, Electrostatic interactions to modulate the reflective assembly of nanoparticles at the oil–water interface, Soft Matter. 8 (2012) 11923–11932. doi:10.1039/c2sm26890f.

[72] Y.K. Park, S.H. Yoo, S. Park, Assembly of highly ordered nanoparticle monolayers at a water/ hexane interface, Langmuir. 23 (2007) 10505–10510. doi:10.1021/la701445a.
[73] Y.-K. Park, S. Park, Directing Close-Packing of Midnanosized Gold Nanoparticles at a Water/Hexane Interface, Chem. Mater. 20 (2008) 2388–2393. doi:10.1021/cm703498y.
[74] F. Ciesa, A. Plech, Gold nanoparticle membranes as large-area surface monolayers, J. Colloid Interface Sci. 346 (2010) 1–7. doi:10.1016/j.jcis.2010.02.030.
[75] T. Ding, A.W. Rudrum, L.O. Herrmann, V. Turek, J.J. Baumberg, Polymer-assisted self-assembly of gold nanoparticle monolayers and their dynamical switching, Nanoscale. 8 (2016) 15864–15869. doi:10.1039/C6NR05199E.
[76] Y.-J. Li, W.-J. Huang, S.-G. Sun, A Universal Approach for the Self-Assembly of Hydrophilic Nanoparticles into Ordered Monolayer Films at a Toluene/Water Interface, Angew. Chemie Int. Ed. 45 (2006) 2537–2539. doi:10.1002/anie.200504595.
[77] N. Younan, M. Hojeij, L. Ribeaucourt, H.H. Girault, Electrochemical properties of gold nanoparticles assembly at polarised liquid|liquid interfaces, Electrochem. Commun. 12 (2010) 912–915. doi:10.1016/j.elecom.2010.04.019.
[78] M. Hojeij, N. Younan, L. Ribeaucourt, H.H. Girault, Surface plasmon resonance of gold nanoparticles assemblies at liquid | liquid interfaces., Nanoscale. 2 (2010) 1665–1669. doi:10.1039/c0nr00241k.
[79] P. Fang, S. Chen, H. Deng, M.D. Scanlon, F. Gumy, H.J. Lee, D. Momotenko, V. Amstutz, F. Cortés-Salazar, C.M. Pereira, Z. Yang, H.H. Girault, Conductive Gold Nanoparticle Mirrors at Liquid/Liquid Interfaces, ACS Nano. 7 (2013) 9241–9248. doi:10.1021/nn403879g.
[80] G. Vazquez, E. Alvarez, J.M. Navaza, Surface Tension of Alcohol Water + Water from 20 to 50 .degree.C, J. Chem. Eng. Data. 40 (1995) 611–614. doi:10.1021/je00019a016.
[81] M. Luo, Y. Song, L.L. Dai, Effects of methanol on nanoparticle self-assembly at liquid-liquid interfaces: A molecular dynamics approach, J. Chem. Phys. 131 (2009) 194703. doi:10.1063/1.3258344.
[82] H. Xia, D. Wang, Fabrication of macroscopic freestanding films of metallic nanoparticle monolayers by interfacial self-assembly, Adv. Mater. 20 (2008) 4253–4256. doi:10.1002/adma.200702978.
[83] E. Smirnov, Assemblies of gold nanoparticles at liquid-liquid interfaces : from liquid optics to electrocatalysis, Ecole Polytechnique Fédérale de Lausanne, 2017.
[84] B. Su, J.-P. Abid, D.J. Fermín, H.H. Girault, H. Hoffmannová, P. Krtil, Z. Samec, Reversible Voltage-Induced Assembly of Au Nanoparticles at Liquid|Liquid Interfaces, J. Am. Chem. Soc. 126 (2004) 915–919. doi:10.1021/ja0386187.
[85] J.P. Abid, M. Abid, C. Bauer, H.H. Girault, P.F. Brevet, Controlled reversible adsorption of core-shell metallic nanoparticles at the polarized water/1,2-dichloroethane interface investigated by optical second-harmonic generation, J. Phys. Chem. C. 111 (2007) 8849–8855. doi:10.1021/jp067181x.
[86] J.-Y. Kim, N.A. Kotov, Charge Transport Dilemma of Solution-Processed Nanomaterials, Chem. Mater. 26 (2014) 134–152. doi:10.1021/cm402675k.
[87] W.P. Wuelfing, S.J. Green, J.J. Pietron, D.E. Cliffel, R.W. Murray, C. Hill, N. Carolina, R. V June, V. Re, M. Recei, V. September, Electronic Conductivity of Solid-State , Mixed-Valent , Monolayer-Protected Au Clusters, J. Am. Chem. Soc. 122 (2000) 11465–11472. doi:10.1021/ja002367+.
[88] A.N.J. Rodgers, R.A.W. Dryfe, Oxygen Reduction at the Liquid-Liquid Interface: Bipolar Electrochemistry through Adsorbed Graphene Layers, ChemElectroChem. 3 (2016) 472–479. doi:10.1002/celc.201500343.
[89] P.S. Toth, Q.M. Ramasse, M. Velický, R. a. W. Dryfe, Functionalization of graphene at the organic/water interface, Chem. Sci. 6 (2015) 1316–1323. doi:10.1039/C4SC03504F.

[90] P.S. Toth, A.N.J. Rodgers, A.K. Rabiu, R.A.W. Dryfe, Electrochemical activity and metal deposition using few-layer graphene and carbon nanotubes assembled at the liquid-liquid interface, Electrochem. Commun. 50 (2015) 6–10. doi:10.1016/j.elecom.2014.10.010.
[91] S. Rastgar, H. Deng, F. Cortés-Salazar, M.D. Scanlon, M. Pribil, V. Amstutz, A.A. Karyakin, S. Shahrokhian, H.H. Girault, Oxygen reduction at soft interfaces catalyzed by in situ-generated reduced graphene oxide, ChemElectroChem. 1 (2014) 59–63. doi:10.1002/celc.201300140.
[92] P. Ge, M.D. Scanlon, P. Peljo, X. Bian, H. Vubrel, A. O'Neill, J.N. Coleman, M. Cantoni, X. Hu, K. Kontturi, B. Liu, H.H. Girault, Hydrogen evolution across nano-Schottky junctions at carbon supported MoS2 catalysts in biphasic liquid systems, Chem. Commun. 48 (2012) 6484–6486. doi:10.1039/c2cc31398g.
[93] X. Bian, M.D. Scanlon, S. Wang, L. Liao, Y. Tang, B. Liu, H.H. Girault, Floating conductive catalytic nano-rafts at soft interfaces for hydrogen evolution, Chem. Sci. 4 (2013) 3432–3441. doi:10.1039/C3SC51290H.
[94] P.K. Jain, M.A. El-Sayed, Noble metal nanoparticle Pairs: Effect of medium for enhanced nanosensing, Nano Lett. 8 (2008) 4347–4352. doi:10.1021/nl8021835.
[95] P.K. Jain, M.A. El-Sayed, Plasmonic coupling in noble metal nanostructures, Chem. Phys. Lett. 487 (2010) 153–164. doi:10.1016/j.cplett.2010.01.062.
[96] L. Velleman, D. Sikdar, V.A. Turek, A.R. Kucernak, S.J. Roser, A.A. Kornyshev, J.B. Edel, Tuneable 2D self-assembly of plasmonic nanoparticles at liquid|liquid interfaces, Nanoscale. 8 (2016) 19229–19241. doi:10.1039/C6NR05081F.
[97] H.H. Girault, D.J. Schiffrin, B.D.V. Smith, Drop image processing for surface and interfacial tension measurements, J. Electroanal. Chem. 137 (1982) 207–217. doi:10.1016/0022-0728(82)80036-3.
[98] H.H.J. Girault, D.J. Schiffrin, B.D. V Smith, The measurement of interfacial tension of pendant drops using a video image profile digitizer, J. Colloid Interface Sci. 101 (1984) 257–266. doi:10.1016/0021-9797(84)90026-2.
[99] M.C. Martins, C.M. Pereira, H.H. Girault, F. Silva, Specific adsorption of tetraalkylammonium cations on the 1,2-dicloroethane/water interface, Electrochim. Acta. 50 (2004) 135–139. doi:10.1016/j.electacta.2004.07.023.
[100] M.A. Fernandez-Rodriguez, Y. Song, M.Á. Rodríguez-Valverde, S. Chen, M.A. Cabrerizo-Vilchez, R. Hidalgo-Alvarez, Comparison of the interfacial activity between homogeneous and Janus gold nanoparticles by pendant drop tensiometry, Langmuir. 30 (2014) 1799–1804. doi:10.1021/la404194e.
[101] M.A. Fernández-Rodríguez, A.M. Percebom, J.J. Giner-Casares, M.A. Rodríguez-Valverde, M.A. Cabrerizo-Vílchez, L.M. Liz-Marzán, R. Hidalgo-Álvarez, Interfacial Activity of Gold Nanoparticles Coated with a Polymeric Patchy Shell and the Role of Spreading Agents, ACS Omega. 1 (2016) 311–317. doi:10.1021/acsomega.6b00131.
[102] M.A. Fernandez-Rodriguez, J. Ramos, L. Isa, M.A. Rodriguez-Valverde, M.A. Cabrerizo-Vilchez, R. Hidalgo-Alvarez, Interfacial Activity and Contact Angle of Homogeneous, Functionalized, and Janus Nanoparticles at the Water/Decane Interface, Langmuir. 31 (2015) 8818–8823. doi:10.1021/acs.langmuir.5b02137.
[103] M. Marinescu, M. Urbakh, A.A. Kornyshev, Voltage-dependent capacitance of metallic nanoparticles at a liquid/liquid interface, Phys. Chem. Chem. Phys. 14 (2012) 1371–1380. doi:10.1039/C1CP22937K.
[104] A.J. Olaya, P.-F. Brevet, E.A. Smirnov, H.H. Girault, Ultrafast Population Dynamics of Surface-Active Dyes during Electrochemically Controlled Ion Transfer across a Liquid|Liquid Interface, J. Phys. Chem. C. 118 (2014) 25027–25031. doi:10.1021/jp507585a.
[105] P. Galletto, H.H. Girault, C. Gomis-Bas, D.J. Schiffrin, R. Antoine, M. Broyer, P.F. Brevet, Second harmonic generation response by gold nanoparticles at the polarized water/2-octanone

interface: from dispersed to aggregated particles, J. Phys. Condens. Matter. 19 (2007) 375108. doi:10.1088/0953-8984/19/37/375108.
[106] M. Zanini, L. Isa, Particle contact angles at fluid interfaces: Pushing the boundary bayond hard uniform spherical colloids, J. Phys. Condens. Matter. 53 (2016) 313002. doi:10.1017/CBO9781107415324.004.
[107] A. Maestro, E. Guzmán, F. Ortega, R.G. Rubio, Contact angle of micro- and nanoparticles at fluid interfaces, Curr. Opin. Colloid Interface Sci. 19 (2014) 355–367. doi:10.1016/j.cocis.2014.04.008.
[108] L. Isa, Freeze-fracture Shadow-casting (FreSCa) Cryo-SEM as a Tool to Investigate the Wetting of Micro- and Nanoparticies at Liquid-Liquid Interfaces, Chimia 67 (2013) 231–235. doi:10.2533/chimia.2013.231.
[109] L. Isa, F. Lucas, R. Wepf, E. Reimhult, Measuring single-nanoparticle wetting properties by freeze-fracture shadow-casting cryo-scanning electron microscopy, Nat. Commun. 2 (2011) 438. doi:10.1038/ncomms1441.
[110] O.J. Cayre, V.N. Paunov, Contact angles of colloid silica and gold particles at air-water and oil-water interfaces determined with the gel trapping technique, Langmuir. 20 (2004) 9594–9599. doi:10.1021/la0489615.
[111] L. Costa, G. Li-Destri, N.H. Thomson, O. Konovalov, D. Pontoni, Real Space Imaging of Nanoparticle Assembly at Liquid–Liquid Interfaces with Nanoscale Resolution, Nano Lett. 16 (2016) 5463–5468. doi:10.1021/acs.nanolett.6b01877.
[112] S. Kubowicz, M. a Hartmann, J. Daillant, M.K. Sanyal, V. V Agrawal, C. Blot, O. Konovalov, H. Möhwald, Gold Nanoparticles at the Liquid−Liquid Interface: X-ray Study and Monte Carlo Simulation, Langmuir. 25 (2009) 952–958. doi:10.1021/la802837k.
[113] M.K. Sanyal, V. V. Agrawal, M.K. Bera, K.P. Kalyanikutty, J. Daillant, C. Blot, S. Kubowicz, O. Konovalov, C.N.R. Rao, Formation and Ordering of Gold Nanoparticles at the Toluene−Water Interface, J. Phys. Chem. C. 112 (2008) 1739–1743. doi:10.1021/jp710635e.
[114] N. Laanait, M. Mihaylov, B. Hou, H. Yu, P. Vanýsek, M. Meron, B. Lin, I. Benjamin, M.L. Schlossman, Tuning ion correlations at an electrified soft interface, Proc. Natl. Acad. Sci. 109 (2012) 20326–20331. doi:10.1073/pnas.1214204109.
[115] B. Hou, N. Laanait, H. Yu, W. Bu, J. Yoon, B. Lin, M. Meron, G. Luo, P. Vanysek, M.L. Schlossman, Ion distributions at the water/1,2-dichloroethane interface: Potential of mean force approach to analyzing X-ray reflectivity and interfacial tension measurements, J. Phys. Chem. B. 117 (2013) 5365–5378. doi:10.1021/jp401892y.
[116] I. Cohanoschi, A. Thibert, C. Toro, S. Zou, F.E. Hernández, Surface plasmon enhancement at a liquid-metal-liquid interface, Plasmonics. 2 (2007) 89–94. doi:10.1007/s11468-007-9030-2.
[117] S. Rastgar, M. Pilarski, G. Wittstock, Polarized liquid-liquid interface meets visible light-driven catalytic water oxidation, Chem. Commun. 52 (2016) 11382–11385. doi:10.1039/C6CC04275A.
[118] C. Amatore, J.M. Savéant, D. Tessier, Charge Transfer at Partially Blocked Surfaces - A Model for the Case of Microscopic Active and Inactive Sites, J. Electroanal. Chem. 147 (1983) 39–51. doi:10.1016/S0022-0728(83)80055-2.
[119] A.J. Bard, L.R. Faulkner, Electroactive layers and modified electrodes, in: Electrochemical Methods: Fundamentals and Applications, 2nd ed., John Wiley & Sons, Inc, 2001: pp. 580–631.
[120] P. Zheng, S.K. Cushing, S. Suri, N. Wu, Tailoring plasmonic properties of gold nanohole arrays for surface-enhanced Raman scattering, Phys. Chem. Chem. Phys. 17 (2015) 21211–21219. doi:10.1039/C4CP05291A.
[121] P.N. Bartlett, J.J. Baumberg, S. Coyle, M.E. Abdelsalam, Optical properties of nanostructured metal films, Faraday Discuss. 125 (2004) 117–132. doi:10.1039/b304116f.
[122] J.C. Hulteen, Nanosphere lithography: A materials general fabrication process for periodic particle array surfaces, J. Vac. Sci. Technol. A Vacuum, Surfaces, Film. 13 (1995) 1553–1558.

doi:10.1116/1.579726.
[123] X. Zhang, E.M. Hicks, J. Zhao, G.C. Schatz, R.P. Van Duyne, Electrochemical tuning of silver nanoparticles fabricated by nanosphere lithography, Nano Lett. 5 (2005) 1503–1507. doi:10.1021/nl050873x.
[124] P.-P. Fang, J.-F. Li, Z.-L. Yang, L.-M. Li, B. Ren, Z.-Q. Tian, Optimization of SERS activities of gold nanoparticles and gold-core-palladium-shell nanoparticles by controlling size and shell thickness, J. Raman Spectrosc. 39 (2008) 1679–1687. doi:10.1002/jrs.2066.
[125] A.J. Wilson, K.A. Willets, Visualizing site-specific redox potentials on the surface of plasmonic nanoparticle aggregates with superlocalization SERS microscopy, Nano Lett. 14 (2014) 939–945. doi:10.1021/nl404347a.
[126] A.J. Wain, M.A. O'Connell, Advances in surface-enhanced vibrational spectroscopy at electrochemical interfaces, Adv. Phys. X. 2 (2017) 188–209. doi:10.1080/23746149.2016.1268931.
[127] D.-Y. Wu, J.-F. Li, B. Ren, Z.-Q. Tian, Electrochemical surface-enhanced Raman spectroscopy of nanostructures., Chem. Soc. Rev. 37 (2008) 1025–1041. doi:10.1039/b707872m.
[128] S. Zaleski, A.J. Wilson, M. Mattei, X. Chen, G. Goubert, M.F. Cardinal, K.A. Willets, R.P. Van Duyne, Investigating Nanoscale Electrochemistry with Surface- and Tip-Enhanced Raman Spectroscopy, Acc. Chem. Res. 49 (2016) 2023–2030. doi:10.1021/acs.accounts.6b00327.
[129] A.J. Wilson, N.Y. Molina, K.A. Willets, Modification of the Electrochemical Properties of Nile Blue through Covalent Attachment to Gold As Revealed by Electrochemistry and SERS, J. Phys. Chem. C. 120 (2016) 21091–21098. doi:10.1021/acs.jpcc.6b03962.
[130] A.J. Wilson, K.A. Willets, Unforeseen distance-dependent SERS spectroelectrochemistry from surface-tethered Nile Blue: the role of molecular orientation, Analyst. 141 (2016) 5144–5151. doi:10.1039/C6AN01266C.
[131] C. Zong, C.J. Chen, M. Zhang, D.Y. Wu, B. Ren, Transient Electrochemical Surface-Enhanced Raman Spectroscopy: A Millisecond Time-Resolved Study of an Electrochemical Redox Process, J. Am. Chem. Soc. 137 (2015) 11768–11774. doi:10.1021/jacs.5b07197.
[132] M.G. Millyard, F. Min Huang, R. White, E. Spigone, J. Kivioja, J.J. Baumberg, Stretch-induced plasmonic anisotropy of self-assembled gold nanoparticle mats, Appl. Phys. Lett. 100 (2012) 2012–2015. doi:10.1063/1.3683535.
[133] P. Guo, D. Sikdar, X. Huang, K.J. Si, B. Su, Y. Chen, W. Xiong, L.W. Yap, M. Premaratne, W. Cheng, Large-Scale Self-Assembly and Stretch-Induced Plasmonic Properties of Core–Shell Metal Nanoparticle Superlattice Sheets, J. Phys. Chem. C. 118 (2014) 26816–26824. doi:10.1021/jp508108a.
[134] P. Guo, X. Huang, L. Li, S. Zhao, Interfacial self-assembly approach of plasmonic nanostructures for efficient SERS and recyclable catalysts applications, Chem. Res. Chinese Univ. 33 (2017) 135–142. doi:10.1007/s40242-017-6034-0.
[135] B. Zhou, X. Li, X. Tang, P. Li, L. Yang, J. Liu, Highly Selective and Repeatable Surface-Enhanced Resonance Raman Scattering Detection for Epinephrine in Serum Based on Interface Self-Assembled 2D Nanoparticles Arrays, ACS Appl. Mater. Interfaces. (2017). doi:10.1021/acsami.6b15205.
[136] L. Yan, K. Zhang, H. Xu, J. Ji, Y. Wang, B. Liu, P. Yang, Target induced interfacial self-assembly of nanoparticles: A new platform for reproducible quantification of copper ions, Talanta. 158 (2016) 254–261. doi:10.1016/j.talanta.2016.05.054.
[137] X. Yin, Y. Peretz, P.G. Oppenheimer, L. Zeiri, A. Masarwa, N. Froumin, R. Jelinek, Conductive and SERS-active colloidal gold films spontaneously formed at a liquid/liquid interface, RSC Adv. 6 (2016) 33326–33331. doi:10.1039/C6RA03403A.
[138] X. Lin, W.-L.-J. Hasi, S.-Q.-G.-W. Han, X.-T. Lou, D.-Y. Lin, Z.-W. Lu, Fabrication of transparent SERS

platform via interface self-assembly of gold nanorods and gel trapping technique for on-site real time detection, Phys. Chem. Chem. Phys. 17 (2015) 31324–31331. doi:10.1039/C5CP04828A.
[139] K. Zhang, J. Zhao, H. Xu, Y. Li, J. Ji, B. Liu, Multifunctional Paper Strip Based on Self-Assembled Interfacial Plasmonic Nanoparticle Arrays for Sensitive SERS Detection, ACS Appl. Mater. Interfaces. 7 (2015) 16767–16774. doi:10.1021/acsami.5b04534.
[140] K. Zhang, J. Zhao, J. Ji, Y. Li, B. Liu, Quantitative Label-Free and Real-Time Surface-Enhanced Raman Scattering Monitoring of Reaction Kinetics Using Self-Assembled Bifunctional Nanoparticle Arrays, Anal. Chem. 87 (2015) 8702–8708. doi:10.1021/acs.analchem.5b01406.
[141] K. Zhang, J. Ji, Y. Li, B. Liu, Interfacial Self-Assembled Functional Nanoparticle Array: A Facile Surface-Enhanced Raman Scattering Sensor for Specific Detection of Trace Analytes, Anal. Chem. 86 (2014) 6660–6665. doi:10.1021/ac501383x.
[142] S. Yamamoto, H. Watarai, Surface-Enhanced Raman Spectroscopy of Dodecanethiol-Bound Silver Nanoparticles at the Liquid/Liquid Interface, Langmuir. 22 (2006) 6562–6569. doi:10.1021/la0603119.
[143] M.P. Cecchini, V.A. Turek, J. Paget, A.A. Kornyshev, J.B. Edel, Self-assembled nanoparticle arrays for multiphase trace analyte detection, Nat. Mater. 12 (2012) 165–171. doi:10.1038/nmat3488.
[144] K. Kim, H.S. Han, I. Choi, C. Lee, S. Hong, S.-H. Suh, L.P. Lee, T. Kang, Interfacial liquid-state surface-enhanced Raman spectroscopy, Nat. Commun. 4 (2013) 1–9. doi:10.1038/ncomms3182.
[145] M.P. Cecchini, V.A. Turek, A. Demetriadou, G. Britovsek, T. Welton, A.A. Kornyshev, J.D.E.T. Wilton-Ely, J.B. Edel, Heavy Metal Sensing Using Self-Assembled Nanoparticles at a Liquid-Liquid Interface, Adv. Opt. Mater. 2 (2014) 966–977. doi:10.1002/adom.201400211.
[146] M. Wang, Z. Zhang, J. He, A SERS Study on the Assembly Behavior of Gold Nanoparticles at the Oil/Water Interface, Langmuir. 31 (2015) 12911–12919. doi:10.1021/acs.langmuir.5b03131.
[147] S.G. Booth, D.P. Cowcher, R. Goodacre, R.A.W. Dryfe, Electrochemical modulation of SERS at the liquid/liquid interface., Chem. Commun. 50 (2014) 4482–4484. doi:10.1039/c4cc00359d.
[148] V. Sashuk, K. Winkler, A. Żywociński, T. Wojciechowski, E. Górecka, M. Fiałkowski, Nanoparticles in a capillary trap: Dynamic self-assembly at fluid interfaces, ACS Nano. 7 (2013) 8833–8839. doi:10.1021/nn403297f.
[149] T. Kakiuchi, Electrochemical instability of the liquid|liquid interface in the presence of ionic surfactant adsorption, J. Electroanal. Chem. 536 (2002) 63–69. doi:10.1016/S0022-0728(02)01204-4.
[150] L. Zhang, Y. Kitazumi, T. Kakiuchi, Potential-dependent adsorption and transfer of poly(diallyldialkylammonium) ions at the nitrobenzene|water interface, Langmuir. 27 (2011) 13037–13042. doi:10.1021/la2028077.
[151] Y. Kitazumi, T. Kakiuchi, Imaging of the liquid-liquid interface under electrochemical instability using confocal fluorescence microscopy, Langmuir. 25 (2009) 10829–10833. doi:10.1021/la901374f.